

# Critical fluid dynamics in two and three dimensions

Chandroday Chattopadhyay<sup>1</sup>, Josh Ott<sup>1</sup>, Thomas Schäfer<sup>1</sup>, and Vladimir V. Skokov<sup>1</sup>

<sup>1</sup> *Department of Physics, North Carolina State University, Raleigh, NC 27695*

## Abstract

We describe a numerical method for simulating stochastic fluid dynamics near a critical point in the Ising universality class. This theory is known as model H, and is expected to govern the non-equilibrium dynamics of Quantum Chromodynamics (QCD) near a possible critical endpoint of the phase transition between a hadron liquid and the quark-gluon plasma. The numerical algorithm is based on a Metropolis scheme, and automatically ensures that the distribution function of the hydrodynamic variables in equilibrium is independent of the transport coefficients and only governed by the microscopic free energy. We verify dynamic scaling near the critical point of a two and three-dimensional fluid and extract the associated critical exponent  $z$ . We find  $z \simeq 3$  in three dimensions, and  $z \simeq 2$  for a two-dimensional fluid. In a finite system, we observe a crossover between the mean field value  $z = 4$  and the true critical exponent  $z \simeq 3$  ( $z \simeq 2$  in  $d = 2$ ). This crossover is governed by the values of the correlation length and the renormalized shear viscosity.

## I. INTRODUCTION

Hydrodynamics provides a remarkably effective theory of many strongly interacting fluids [1–3]. This description is based on a set of partial differential equations that express the conservation laws for energy, momentum, and other conserved densities. In the long-wavelength limit the precise form of these differential equations can be constructed order by order as an expansion in derivatives of local thermodynamic variables.

It has been understood for some time that this description is not complete and that fluctuations in the conserved densities and currents cannot be ignored [4, 5]. Indeed, stochastic terms in the conserved currents are constrained by fluctuation-dissipation relations, and they cannot be zero unless the temperature or the dissipative coefficients vanish. Recent work on effective actions defined on the Keldysh contour has demonstrated that stochastic hydrodynamic theories provide a systematically improvable framework for the calculation of correlation functions in the long-wavelength limit [6–11].

At a generic point in the phase diagram, fluctuations lead to non-analytic terms in the low frequency, small momentum expansion of correlation and response functions. These contributions are known as long-time tails. They are very interesting, but in typical fluids they are not easy to observe. In the vicinity of a second-order phase transition, on the other hand, fluctuations are large. In particular, stochastic terms in the hydrodynamic equations account for the divergent correlation length and susceptibilities, and describe the phenomenon of dynamic scaling [12].

Stochastic hydrodynamic theories were classified in the work by Hohenberg and Halperin [12]. This classification includes purely relaxational theories (model A), critical diffusion (model B), critical anti-ferromagnets (model G), and critical diffusion coupled to the Navier-Stokes equation (model H). The last two theories are expected to be relevant to QCD. Model G accounts for the dynamics of the chiral phase transition [13], and model H describes the dynamics near the endpoint of the nuclear liquid-gas transition, as well as a possible critical endpoint of the quark-gluon plasma (QGP) phase transition [14].

The dynamics near a critical endpoint is genuinely non-perturbative – there are no small parameters. Historically, the main approach to the calculation of dynamical critical exponents has been the  $\epsilon$ -expansion. For the models considered here, this is an expansion in  $\epsilon = 4 - d$ , where  $d$  is the number of spatial dimensions [12]. This parameter is not small,

but comparison of the results with experimental data on liquids is encouraging [15]. More recently, a number of groups have used the functional renormalization group [16–22]. For three-dimensional systems, the results are generally consistent with predictions obtained in the  $\epsilon$ -expansion.

These methods have some disadvantages. Up to this point, both the  $\epsilon$ -expansion and the functional renormalization group calculations have been performed at a rather low order of the corresponding truncations. More importantly, it is not obvious how to apply these methods to problems such as heavy-ion collisions that involve a non-trivial background flow. There are a number of recent studies that address critical dynamics in expanding fluids. A typical approach is to consider a non-critical fluid and derive a set of deterministic equations for the equal-time  $n$ -point functions of the theory [23–30]. Critical effects can be taken into account by replacing the susceptibilities and relaxation rates with their critical counterparts.

Despite all these efforts, there have been remarkably few attempts at direct simulation of stochastic hydrodynamic theories. This is not necessarily because of a lack of interest, but because numerical simulations encounter several problems. This includes the fact that short-distance noise requires regularization and renormalization, the importance of implementing a scheme that respects fluctuation-dissipation relations, and the need to resolve ambiguities in the definition of stochastic partial differential equations.

Previous numerical work on stochastic fluid dynamics in a regime in which fluctuations are approximately described by the linearized theory includes Refs. [31–35]. Classical statistical simulations are described in [36–38]. There have also been numerical studies of one-dimensional stochastic diffusion in a system that with longitudinal expansion that traverses the critical regime [39, 40]. Finally, it is possible to use molecular dynamics with a classical Hamiltonian (for example a Lennard-Jones potential) that describes a fluid with a liquid and gas phase [41, 42]. Simulations in the vicinity of the critical end point have been used to verify the critical divergence of the thermal conductivity predicted by the  $\epsilon$ -expansion [42]. However, while stochastic fluid dynamics emerges from the microscopic simulation near the critical point, it is difficult to implement an arbitrary equation of state, or a general set of transport coefficients.

A new approach to simulating stochastic fluid dynamics based on a Metropolis method is discussed in Refs. [43–48]. This method has been utilized in the mathematical literature on stochastic partial differential equations [49], but it does not appear to be widely used. The

idea is to combine the diffusive and stochastic terms in the equation of motion into a single Metropolis step. The advantage of this method is that fluctuation-dissipation relations are automatically satisfied, and that the equilibrium distribution of the hydrodynamic variables is guaranteed to be controlled by the microscopic free energy functional. In a companion paper [48] we have presented the first numerical calculation of the relaxation rate and the dynamic critical exponent in model H. In the present work, we provide a detailed description of the algorithm and numerical details, consistency checks, and further applications to two-dimensional fluids.

## II. STOCHASTIC FLUID DYNAMICS

### A. Definition of Model H

We consider the long-time, fluid dynamic description of a conserved order parameter density  $\phi$  interacting with the momentum density  $\vec{\pi}$  of the fluid. This theory is known as Model H in the classification of Hohenberg and Halperin [12, 50]. The equations of motion are

$$\partial_t \phi = \Gamma \nabla^2 \left( \frac{\delta \mathcal{H}}{\delta \phi} \right) - (\nabla_i \phi) \frac{\delta \mathcal{H}}{\delta \pi_i^T} + \zeta, \quad (1)$$

$$\partial_t \pi_i^T = \eta \nabla^2 \left( \frac{\delta \mathcal{H}}{\delta \pi_i^T} \right) + P_{ij}^T \left[ (\nabla_j \phi) \frac{\delta \mathcal{H}}{\delta \phi} \right] - P_{ij}^T \left[ \nabla_k \left( \pi_j^T \frac{\delta \mathcal{H}}{\delta \pi_k^T} \right) \right] + \xi_i. \quad (2)$$

Here,  $\Gamma$  and  $\eta$  are transport coefficients. In the context of describing the dynamics near a liquid-gas endpoint we can take  $\phi$  to be the specific entropy  $s/n$  of the fluid [27, 51],  $\Gamma$  is the thermal diffusivity, and  $\eta$  is the shear viscosity. The transverse projection operator is given by

$$P_{ij}^T = \delta_{ij} - \frac{\nabla_i \nabla_j}{\nabla^2} \quad (3)$$

and  $\pi_i^T = P_{ij}^T \pi_j$ . The effective Hamiltonian is given by

$$\mathcal{H} = \int d^d x \left[ \frac{1}{2\rho} (\pi_i^T)^2 + \frac{1}{2} (\nabla \phi)^2 + \frac{1}{2} m^2 \phi^2 + \frac{1}{4} \lambda \phi^4 - h \phi \right], \quad (4)$$

where  $\rho$  is the mass density,  $m$  is the inverse correlation length,  $\lambda$  is a non-linear self-coupling, and  $h$  is an external field. In order to describe a possible critical endpoint in the QCD phase diagram we identify  $\rho$  with the enthalpy density of the fluid, and we map the parameters

$m^2$ ,  $h$ , and  $\lambda$  onto the chemical potential-temperature  $(\mu, T)$  plane of QCD, see for example [52, 53]. The noise terms  $\zeta$  and  $\xi_i$  are random fields constrained by fluctuation-dissipation relations. The correlation functions of the noise are given by

$$\langle \zeta(t, \vec{x}) \zeta(t', \vec{x}') \rangle = -2T \Gamma \nabla^2 \delta(\vec{x} - \vec{x}') \delta(t - t'), \quad (5)$$

$$\langle \xi_i(t, \vec{x}) \xi_j(t', \vec{x}') \rangle = -2T \eta P_{ij}^T \nabla^2 \delta(\vec{x} - \vec{x}') \delta(t - t'). \quad (6)$$

## B. Shear vs sound

The hydrodynamic equations (1,2) describe the interaction of shear modes with the order parameter, but they do not include sound modes. This is based on the observation that in order to study critical dynamics we can focus on the long-time behavior of the fluid, governed by modes with the lowest frequency. Shear modes have a dispersion relation  $\omega \simeq i(\eta/\rho)k^2$ , whereas sound modes are described by  $\omega \simeq c_s k$ , where  $c_s$  is the speed of sound. This means that at long distances (or low wave numbers) the magnitude of the frequency of shear waves is smaller than that of sound waves.

There are, however, phenomena that require the inclusion of sound modes. One of them is the critical behavior of the bulk viscosity, which is given by  $\zeta \sim \xi^{z-\alpha/\nu}$ , where  $\xi$  is the correlation length,  $z \simeq 3.05$  is the dynamic exponent,  $\alpha \simeq 0.11$  is the specific heat exponent,  $\nu \simeq 0.63$  is the correlation length exponent [54, 55]. Another is the dispersion relation of sound itself. Near the critical point the speed of sound vanishes as  $c_s^2 \sim \xi^{-\alpha/\nu}$ , but finite frequency modes propagate with a finite speed, governed by a universal function [56, 57].

Projecting on the transverse component of the momentum density is useful, because the longitudinal part of  $\vec{\pi}$  couples to the energy density  $\mathcal{E}$  and pressure  $P$  of the fluid. This means that if  $\vec{\pi}_L$  is included we also have to include an equation of motion for the energy density, and we have to study the renormalization of the equation of state by short distance fluctuations. We also observe that the projection on transverse modes simplifies the mode coupling between  $\vec{\pi}$  and  $\phi$ . In particular,  $(\nabla_j \phi) V'(\phi) = \nabla_j V(\phi)$  is longitudinal, so that only the gradient term in  $\mathcal{H}(\phi)$  contributes to the mode-coupling between  $\vec{\pi}$  and  $\phi$ .

Different authors define model H in slightly different ways. For example, Hohenberg and Halperin [12] only consider the two mode-coupling terms between  $\phi$  and  $\vec{\pi}$ , but not the mode-coupling of  $\vec{\pi}$  with itself. Obviously, we need the first type of coupling, because otherwise there is no interaction between the two types of fluctuations. Also, we have to

include both the coupling of  $\vec{\pi}^T$  to  $\phi$  and its reverse in order to ensure that the system can equilibrate. The argument for neglecting the self-coupling of  $\vec{\pi}^T$  is based on the observation that fluctuations of  $\vec{\pi}^T$  are damped as  $(\eta/\rho)k^2$ , whereas critical fluctuations of  $\phi$  are much more weakly damped, proportional to  $\Gamma k^4$ . Below, we will study the role of the  $\vec{\pi}^T$  self-coupling numerically. We will refer to the theory defined by Eqs. (1,2) as model H, and the theory without the self-coupling as model H0. A complete model H, with sound modes taken into account, was studied in Refs. [58, 59], see also [56, 57].

### C. Conservation laws

Two of the mode-coupling terms have a straightforward interpretation as the advection terms. We can write

$$\partial_t \phi + \frac{1}{\rho} (\pi_i^T \nabla_i) \phi = \Gamma \nabla^2 \frac{\delta \mathcal{H}}{\delta \phi}, \quad (7)$$

$$\partial_t \pi_i^T + \frac{1}{\rho} (\pi_j^T \nabla_j) \pi_i^T = \eta \nabla^2 \frac{\delta \mathcal{H}}{\delta \pi_i^T} + \dots \quad (8)$$

On the other hand, the coupling of  $\vec{\pi}$  to gradients of  $\phi$  does not have a simple interpretation, and it goes beyond the standard Navier-Stokes approximation. However, it is clearly essential in order to guarantee the symmetry of the mode-couplings, and to ensure that energy can be exchanged between  $\phi$  and  $\vec{\pi}$ . This term can be understood more clearly by writing the equations of motion in conservative form

$$\partial_t \phi + \vec{\nabla} \cdot \vec{j} = 0, \quad \partial_t \pi_{T,i} + P_{ij}^T \nabla_k \Pi_{jk} = 0. \quad (9)$$

Here the currents contain non-dissipative as well as a dissipative/stochastic parts

$$j_i = j_i^{(0)} + j_i^{(1)}, \quad \Pi_{ij} = \Pi_{ij}^{(0)} + \Pi_{ij}^{(1)}. \quad (10)$$

The currents are given by

$$j_i^{(0)} = \phi \frac{\delta \mathcal{H}}{\delta \pi_i^T} = \frac{1}{\rho} \phi \pi_i^T, \quad (11)$$

$$j_i^{(1)} = -\Gamma \nabla_i \frac{\delta \mathcal{H}}{\delta \phi} + \theta_i \quad (12)$$

as well as

$$\Pi_{ij}^{(0)} = \frac{1}{\rho} \pi_i^T \pi_j^T + (\nabla_i \phi)(\nabla_j \phi), \quad (13)$$

$$\Pi_{ij}^{(1)} = -\eta \left[ \nabla_i \frac{\delta \mathcal{H}}{\delta \pi_j^T} + \nabla_j \frac{\delta \mathcal{H}}{\delta \pi_i^T} \right] + \Lambda_{ij}, \quad (14)$$

where  $\Theta_i$  and  $\Lambda_{ij}$  are delta correlated noise fields with variance  $\langle \Theta_i \Theta_j \rangle \sim 2\Gamma T \delta_{ij}$  and  $\langle \Lambda_{ij} \Lambda_{kl} \rangle \sim 2\eta T (\delta_{ik} + \delta_{jl})$ , respectively. This form of the equation makes the physical meaning of the mode coupling between  $\partial_t \vec{\pi}$  and  $\nabla_i \phi$  more transparent. It corresponds to including the stress of  $\phi$  in the stress tensor  $\Pi_{ij}$ .

The structure of the mode couplings can also be understood using Poisson brackets [60]. We can define a four-component field  $\psi^a = (\phi, \pi^i)$ . Then, the mode-couplings arise from the Poisson brackets

$$\partial_t \psi^a = \{\mathcal{H}, \psi^a\} = - \int d^3x \{\psi^a, \psi^b\} \frac{\delta \mathcal{H}}{\delta \psi^b} = - \int d^3x Q^{ab} \frac{\delta \mathcal{H}}{\delta \psi^b}, \quad (15)$$

where the fundamental Poisson brackets  $\{\psi^a, \psi^b\}$  are given in [60]. Equation (15) immediately implies that the Hamiltonian is conserved by the mode-coupling terms,  $\partial_t \mathcal{H} = \{\mathcal{H}, \mathcal{H}\} = 0$ . In terms of the equation of motion for  $\psi^a$ , we can view the conservation of  $\mathcal{H}$  as a consequence of the anti-symmetry of  $Q^{ab}$ ,

$$\partial_t \mathcal{H} = \int d^3x \int d^3x' Q^{ab} \frac{\delta \mathcal{H}}{\delta \psi^a} \frac{\delta \mathcal{H}}{\delta \psi^b} = 0. \quad (16)$$

Equation (15) is also useful for deriving a Fokker-Planck equation for the time-evolution of the probability distribution  $P[\psi^a]$ . In particular, the anti-symmetry of  $Q^{ab}$  implies that the Fokker-Planck equation has a stationary solution  $\exp(-\mathcal{H}[\psi]/T)$  [12].

### III. NUMERICAL METHOD

#### A. Lattice formulation

In order to study the theory numerically we discretize the fields  $\phi(\vec{x})$  and  $\vec{\pi}(\vec{x})$  on a  $d$ -dimensional lattice  $\vec{x} = \vec{n}a$  with  $n_i = 1, \dots, N$ . We can define forward and backward derivatives in the direction  $\mu = 1, 2, 3$  as

$$\nabla_\mu^R \phi(\vec{x}) = \frac{1}{a} [\phi(\vec{x} + \hat{\mu}a) - \phi(\vec{x})], \quad \nabla_\mu^L \phi(\vec{x}) = \frac{1}{a} [\phi(\vec{x}) - \phi(\vec{x} - \hat{\mu}a)]. \quad (17)$$

Note that in the actual implementation we set  $a = 1$ . The Laplacian is defined as  $\nabla^2 = \nabla_\mu^L \nabla_\mu^R = \nabla_\mu^R \nabla_\mu^L$  where summation over  $\mu$  is implied. Note that this lattice derivative satisfies integration by parts

$$\sum_{\vec{x}} \nabla_\mu^R \phi(\vec{x}) \nabla_\mu^R \phi(\vec{x}) = - \sum_{\vec{x}} \phi(\vec{x}) \nabla^2 \phi(\vec{x}). \quad (18)$$

Also note that the operators  $\nabla_\mu^{R,L}$  are not anti-hermitian,

$$(\nabla_\mu^R)^\dagger = -\nabla_\mu^L, \quad (\nabla_\mu^L)^\dagger = -\nabla_\mu^R, \quad (19)$$

but their average, the symmetric (centered) difference operator is

$$\nabla_\mu^c = \frac{1}{2} (\nabla_\mu^L + \nabla_\mu^R), \quad (\nabla_\mu^c)^\dagger = -\nabla_\mu^c. \quad (20)$$

We can define a centered Laplacian

$$(\nabla_\nu^c)^2 \phi(\vec{x}) = \frac{1}{4} \sum_\nu \left\{ \phi(\vec{x} + 2\hat{\nu}) + \phi(\vec{x} - 2\hat{\nu}) - 2\phi(\vec{x}) \right\}, \quad (21)$$

We are now in a position to specify the lattice discretized Hamiltonian as

$$\mathcal{H} = \sum_{\vec{x}} \left[ \frac{1}{2\rho} \pi_\mu^T(\vec{x}) \pi_\mu^T(\vec{x}) + \frac{1}{2} \nabla_\mu^R \phi(\vec{x}) \nabla_\mu^R \phi(\vec{x}) + \frac{1}{2} m^2 \phi^2(\vec{x}) + \frac{1}{4} \lambda \phi^4(\vec{x}) \right], \quad (22)$$

where again the sum over  $\mu$  is implied. Below, we will also consider a Hamiltonian where the gradient term is defined in terms of centered derivatives

$$\mathcal{H}_{\partial\phi}^c = \sum_{\vec{x}} \frac{1}{2} \nabla_\mu^c \phi(\vec{x}) \nabla_\mu^c \phi(\vec{x}) = - \sum_{\vec{x}} \frac{1}{2} \phi(\vec{x}) (\nabla^c)^2 \phi(\vec{x}). \quad (23)$$

We define lattice transverse fields using the centered derivative

$$(\nabla^c)^2 \pi_\mu^T(\vec{x}) = ((\nabla^c)^2 \delta_{\mu\nu} - \nabla_\mu^c \nabla_\nu^c) \pi_\nu(\vec{x}). \quad (24)$$

It is possible to define transverse fields using the left and right derivatives, but in that case one has to consider two types of fields, left and right projected transverse momentum densities,  $\nabla_\mu^L \pi_\mu^{T,L} = 0$  and  $\nabla_\mu^R \pi_\mu^{T,R} = 0$ . On a discrete lattice, these fields are not the same.

We can solve for the projected fields using discrete Fourier transforms

$$\tilde{\phi}(\vec{k}) = \sum_{\vec{x}} \phi(\vec{x}) e^{i\vec{k}\cdot\vec{x}}, \quad (25)$$

$$\tilde{\pi}_\mu(\vec{k}) = \sum_{\vec{x}} \pi_\mu(\vec{x}) e^{i\vec{k}\cdot\vec{x}}, \quad (26)$$

where the discrete momenta are given by  $\vec{k} = 2\pi\vec{m}/L$  with  $m_i = 0, \dots, N-1$ . The projected fields are given by  $\tilde{\pi}_\mu^T = P_{\mu\nu}^T \tilde{\pi}_\nu$  with

$$P_{\mu\nu}^T = \delta_{\mu\nu} - \frac{\tilde{k}_\mu \tilde{k}_\nu}{\tilde{k}^2}, \quad \tilde{k}_\mu = \frac{1}{a} \sin(ak_\mu). \quad (27)$$



## B. Advection terms using skew-symmetric derivatives

In solving the equations of motion it is desirable to maintain as many of the conservation laws and symmetries of the continuum formulation as possible. In Sect. II C we showed that the equations can be written in manifestly momentum and charge conserving forms. We also saw that the symplectic structure of the advection term implies the conservation of  $\mathcal{H}$ . It is instructive to see how this works in more detail. In the continuum the advection term for  $(\phi, \vec{\pi}^T)$  is

$$\dot{\phi} = -\nabla_i \left( \phi \frac{\pi_i^T}{\rho} \right) = -\frac{\pi_i^T}{\rho} \nabla_i \phi, \quad (28)$$

$$\begin{aligned} \dot{\pi}_i^T &= -P_{ij}^T \nabla_k \left( \frac{1}{\rho} \pi_k^T \pi_j^T + \nabla_k \phi \nabla_j \phi \right) \\ &= -P_{ij}^T \left[ \nabla_k \left( \frac{1}{\rho} \pi_k^T \pi_j^T \right) + \nabla_j \phi \nabla^2 \phi \right]. \end{aligned} \quad (29)$$

The time derivative of the Hamiltonian is

$$\dot{\mathcal{H}} = \int d^3x \left[ -\dot{\phi} \nabla^2 \phi + \frac{1}{\rho} \pi_i^T \dot{\pi}_i^T + V'(\phi) \dot{\phi} \right]. \quad (30)$$

Substituting the equations of motion (28-29) we obtain

$$\dot{\mathcal{H}} = \int d^3x \left[ (\nabla^2 \phi) \frac{\pi_i^T}{\rho} \nabla_i \phi - \frac{\pi_i^T}{\rho} \left( \frac{\pi_j^T}{\rho} \nabla_j \right) \pi_i^T - (\nabla^2 \phi) \frac{\pi_i^T}{\rho} \nabla_i \phi - \nabla_i \left( V(\phi) \frac{\pi_i^T}{\rho} \right) \right]. \quad (31)$$

The first and third terms cancel each other. The second term can be written as a divergence

$$\frac{\pi_i^T}{\rho} \left( \frac{\pi_j^T}{\rho} \nabla_j \right) \pi_i^T = \nabla_i \left( \frac{\pi_i^T}{\rho} \frac{\pi_j^T \pi_j^T}{2\rho} \right), \quad (32)$$

and the total energy is conserved as long boundary terms can be ignored. However, these manipulations are not necessarily allowed in the discretized theory. This includes the vector identities used in Eq. (32), as well as the integration by parts identities used to simplify the gradient and potential terms for  $\phi$ .

The question to what extent vector identities in the continuum theory can be maintained in a lattice discretized theory was studied systematically by Morinishi et al. [61]. They first observe that among several ways of writing the self-advection term of the momentum density the “skew-symmetric” form

$$\nabla_\mu \left( \frac{1}{\rho} \pi_\mu^T \pi_\nu^T \right) \Big|_{skew} \equiv \frac{1}{2} \nabla_\mu \left( \frac{1}{\rho} \pi_\mu^T \pi_\nu^T \right) + \frac{1}{2} \frac{\pi_\mu^T}{\rho} \nabla_\mu \pi_\nu^T \quad (33)$$

is distinguished by the fact that conservation of kinetic energy holds independent of the continuity relation  $\nabla_k \pi_k^T = 0$ . The second observation is that Eq. (32) can be preserved with a suitable definition of the derivative and the product of two fields. Consider the lattice interpolation of a field  $\phi$

$$\bar{\phi}^{\hat{\mu}} \equiv \frac{1}{2} [\phi(\vec{x} + \hat{\mu}/2) + \psi(\vec{x} - \hat{\mu}/2)], \quad (34)$$

the lattice interpolation of the product of two fields  $\phi$  and  $\psi$

$$(\widetilde{\phi\psi})^{\hat{\mu}} \equiv \frac{1}{2} [\phi(\vec{x} + \hat{\mu}/2) \psi(\vec{x} - \hat{\mu}/2) + \phi(\vec{x} - \hat{\mu}/2) \psi(\vec{x} + \hat{\mu}/2)], \quad (35)$$

as well as the symmetric half-step derivative

$$\nabla_{\mu}^{1/2} \phi(x) = \frac{1}{2} [\phi(x + \hat{\mu}/2) - \phi(x - \hat{\mu}/2)]. \quad (36)$$

Then the following product rule holds

$$\nabla_{\mu}^{1/2} \left( \widetilde{\phi\psi} \right)^{\hat{\mu}} = (\nabla_{\mu}^c \phi) \psi + \phi (\nabla_{\mu}^c \psi), \quad (37)$$

and we can show that

$$\frac{1}{2} \frac{d}{dt} (\pi_{\nu}^T \pi_{\nu}^T) = \pi_{\nu}^T \nabla_{\mu} \left( \frac{1}{\rho} \pi_{\mu}^T \pi_{\nu}^T \right) \Big|_{skew} = \frac{1}{2} \nabla_{\mu}^{1/2} \left[ (\overline{\pi_{\mu}^T})^{\hat{\mu}} (\widetilde{\pi_{\nu}^T \pi_{\nu}^T})^{\hat{\mu}} \right], \quad (38)$$

which ensures that the advection step conserves the kinetic energy of the fluid.

A similar construction is possible for the mutual advection of  $\phi$  and  $\pi$ . That case is more complicated, because the equations of motion contain third derivative terms in  $\phi$ . Also, in the continuum, there are two separate conservation laws. One conserved quantity is the sum  $[(\pi_i^T)^2/\rho + (\nabla_i \phi)^2]/2$ , the other is the potential energy  $V(\phi)$ . On the lattice we can only implement the first of these conservation laws exactly. For this purpose we write the mutual advection terms using centered derivatives

$$\dot{\phi} = -\frac{1}{\rho} \pi_{\mu}^T \nabla_{\mu}^c \phi, \quad \dot{\pi}_{\mu}^T = -(\nabla_{\mu}^c \phi) (\nabla_{\nu}^c \nabla_{\nu}^c \phi), \quad (39)$$

where the centered Laplacian is defined in Eq. (21). The update in Eq. (39) has the property that it conserves the Hamiltonian

$$\mathcal{H}_{\pi} + \mathcal{H}_{\partial\phi}^c = \sum_{\vec{x}} \left[ \frac{1}{2\rho} \pi_{\mu}^T(\vec{x}) \pi_{\mu}^T(\vec{x}) + \frac{1}{2} \nabla_{\mu}^c \phi(\vec{x}) \nabla_{\mu}^c \phi(\vec{x}) \right]. \quad (40)$$

Note that the update does not exactly conserve the potential energy, nor does it conserve the gradient energy of the scalar field computed from forward derivatives, as in Eq. (22) [76]. We will study the effect of this on our numerical simulations in Section III.

In summary, we use the following spatial discretization of the advection step

$$\dot{\phi} = -\frac{1}{\rho} \pi_\mu^T \nabla_\mu^c \phi, \quad (41)$$

$$\dot{\pi}_\mu^T = - \left[ \frac{1}{2} \nabla_\nu^c \left( \frac{1}{\rho} \pi_\nu^T \pi_\mu^T \right) + \frac{1}{2\rho} \pi_\nu^T \nabla_\nu^c \pi_\mu^T + (\nabla_\mu^c \phi) (\nabla_\nu^c \nabla_\nu^c \phi) \right]. \quad (42)$$

This update does not preserve the transversality of  $\pi_\mu^T$ . After each discrete time step (see next section), we apply the transverse projection operator in Eq. (27), which ensures that  $\pi_\mu^T$  is transverse with regard to the centered derivative,  $\nabla_\mu^c \pi_\mu^T(\vec{x}) = 0$ .

### C. Third order Runge-Kutta

We integrate the advection terms Eqs. (41-42) using a Runge-Kutta method. We define a four-component field  $\phi_\mu = (\phi, \vec{\pi}^T)$  and write the evolution equations as

$$\dot{\phi}_\mu = \mathcal{F}_\mu(\phi_\nu). \quad (43)$$

We integrate this equation using the strong stable third order Runge-Kutta (RK3) scheme developed by Shu and Osher [62]. The RK3 scheme is defined by

$$\phi_\mu^{n+1/3} = \phi_\mu^n + \Delta t \mathcal{F}_\mu(\phi_\nu^n), \quad (44)$$

$$\phi_\mu^{n+2/3} = \frac{3}{4} \phi_\mu^n + \frac{1}{4} \phi_\mu^{n+1/3} + \frac{\Delta t}{4} \mathcal{F}_\mu(\phi_\nu^{n+1/3}), \quad (45)$$

$$\phi_\mu^{n+1} = \frac{1}{3} \phi_\mu^n + \frac{2}{3} \phi_\mu^{n+2/3} + \frac{2}{3} \Delta t \mathcal{F}_\mu(\phi_\nu^{n+2/3}). \quad (46)$$

We apply the transverse projector (27) after every substep of the algorithm.

### D. Dissipative update

We perform the dissipative update using the Metropolis algorithm recently studied in Refs. [43–47], see also recent work in the mathematical literature [49]. The basic observation is that the diffusive step and the noise term can be realized by a single Metropolis update. Here, the first moment of the Metropolis step realizes the diffusive step, and the

second moment implements the noise term. By combining the two terms we guarantee that fluctuation-dissipation relations are satisfied, and that the algorithm converges to an equilibrium distribution which only depends on the Hamiltonian, and not on the dissipative coefficients. In equilibrium the probability density of the fields is given by the Gibbs distribution  $P[\phi_\mu] \sim \exp(-\mathcal{H}[\phi_\mu]/T)$ .

The Metropolis update for the field  $\phi$  is identical to the update previously used in model B [46]. We have

$$\phi^{trial}(\vec{x}, t + \Delta t) = \phi(\vec{x}, t) + q_\mu, \quad (47)$$

$$\phi^{trial}(\vec{x} + \hat{\mu}, t + \Delta t) = \phi(\vec{x} + \hat{\mu}, t) - q_\mu, \quad (48)$$

$$q_\mu = \sqrt{2\Gamma T(\Delta t)} \xi, \quad (49)$$

where  $\xi$  is a Gaussian random variable with unit variance and  $\hat{\mu}$  is an elementary lattice vector in the direction  $\mu = 1, \dots, d$ . The update is accepted with probability  $\min(1, e^{-\Delta\mathcal{H}/T})$ . Note that this algorithm is automatically conserving. We follow the same procedure for  $\vec{\pi}$  and perform a trial update

$$\pi_\nu^{trial}(\vec{x}, t + \Delta t) = \pi_\nu(\vec{x}, t) + r_\nu^{(\mu)}, \quad (50)$$

$$\pi_\nu^{trial}(\vec{x} + \hat{\mu}, t + \Delta t) = \pi_\nu(\vec{x} + \hat{\mu}, t) - r_\nu^{(\mu)}, \quad (51)$$

$$r_\nu^{(\mu)} = \sqrt{2\eta T(\Delta t)} \zeta_\nu^{(\mu)}, \quad (52)$$

where  $\zeta_\nu^{(\mu)}$  are Gaussian random variables with  $\langle \zeta_\mu^{(\alpha)} \zeta_\nu^{(\beta)} \rangle = \delta_{\mu\nu} \delta^{\alpha\beta}$ . Again, the update is accepted with probability  $\min(1, e^{-\Delta\mathcal{H}/T})$ . After a complete sweep through the lattice we project on the transverse component of momentum density,  $\pi_\mu^T(\vec{x}, t) = P_{\mu\nu}^T \pi_\nu(\vec{x})$ . The projection is carried out in Fourier space, as described in Sect. III A.

For the Metropolis accept-reject step we have to compute the change in Hamiltonian due to the change in the fields. The change in  $\mathcal{H}$  due a local change in  $\phi$  at  $\vec{x}$  is

$$\begin{aligned} \Delta\mathcal{H}_\phi(\vec{x}) &= d \left[ (\phi^{trial}(\vec{x}))^2 - (\phi(\vec{x}))^2 \right] - (\phi^{trial}(\vec{x}) - \phi(\vec{x})) \sum_{\mu=1}^d [\phi(\vec{x} + \hat{\mu}) + \phi(\vec{x} - \hat{\mu})] \\ &\quad + \frac{1}{2} m^2 \left[ (\phi^{trial}(\vec{x}))^2 - (\phi(\vec{x}))^2 \right] + \frac{1}{4} \lambda \left[ (\phi^{trial}(\vec{x}))^4 - (\phi(\vec{x}))^4 \right]. \end{aligned} \quad (53)$$

Here, we use the lattice Hamiltonian defined in Eq. (22). A conserving update involves the transfer of charge  $q_\mu$  from  $\vec{x} + \hat{\mu}$  to  $\vec{x}$ . The change in  $\mathcal{H}$  is

$$\Delta\mathcal{H}_\phi(\vec{x}, \vec{x} + \hat{\mu}) = \Delta\mathcal{H}_\phi(\vec{x}) + \Delta\mathcal{H}_\phi(\vec{x} + \hat{\mu}) + (q_\mu)^2. \quad (54)$$

The Hamiltonian is local and quadratic in the momentum density. This implies that the change in the Hamiltonian due to a transfer of momentum is particularly simple

$$\Delta\mathcal{H}_\pi(\vec{x}, \vec{x} + \hat{\mu}) = \frac{1}{\rho} \left[ r_\nu^{(\mu)} (\pi_\nu^T(\vec{x}) - \pi_\nu^T(\vec{x} + \hat{\mu})) + (r_\nu^{(\mu)})^2 \right]. \quad (55)$$

The Metropolis updates can be performed on a checkerboard as explained in Ref. [46]. Also note that as described here the timestep  $\Delta t$  for the dissipative update is the same as the timestep in the Runge-Kutta update, but there is no requirement for the two to be the same. Finally, the update of the momentum density does not preserve the transversality of  $\pi_\mu^T$ . After a complete sweep through the lattice we apply the transverse projection operator defined in Eq. (27).

### E. Choice of units

The equations are solved on a spatial lattice with lattice constant  $a$ . In the following we will set  $a = 1$ , and all distances are measured in units of  $a$ . At the critical point the theory is scale invariant, and the value of  $a$  in physical units does not play a role. Away from the critical point the correlation length  $\xi$  in units of  $a$  is finite, and the value of  $\xi$  in QCD (or any other microscopic theory) can be used to fix the value of  $a$  in units of meters. The conductivity  $\Gamma$  has units of  $l^4/t$ , where  $t$  is time and  $l$  is length. We will set  $\Gamma = 1$ , and time is measured in units of  $a^4/\Gamma$ .

The scalar field has units of  $(T_0/a)^{1/2}$ , where  $T_0$  is a temperature (and the Boltzmann constant is set to one). We can adopt the choice of units  $T_0 = 1$  and measure  $\phi$  in units of  $(T_0/a)^{1/2}$ . The momentum density  $\pi$  is then measured in units of  $T_0/\Gamma$ , and the mass (or enthalpy) density is expressed in units of  $\rho_0 = T_0 a^3/\Gamma^2$ . Finally, the viscosity is measured in units of  $\eta_0 = T_0 a/\Gamma$ , and the specific viscosity  $\eta/\rho$  in units of  $\Gamma/a^2$ . Note that we have set  $\Gamma = 1$  by a choice of units, but the dimensionless viscosity and mass density are parameters of our theory.

The free energy density has three additional parameters, the mass  $m$  which is the inverse bare correlation length, the non-linear self coupling  $\lambda$ , and an external field  $h$ . At the critical point the system is universal and we can pick a value of  $\lambda$  and tune to the critical point  $h = 0$  and  $m^2 = m_c^2$ . Away from the critical point  $\lambda$  is a relevant parameter.

Let us provide a simple estimate of “realistic” values of the parameters, which corre-

spond to a quark gluon fluid near a possible critical end point. At the critical point the theory is scale invariant, and the choice of  $a$  is arbitrary. Away from the critical point the renormalization of the viscosity described in Eq. (63) below implies that  $a$  cannot be made arbitrarily small while maintaining the physical value of the shear viscosity. In practice it does not make sense to make  $a$  much smaller than the non-critical value of the correlation length. This quantity is not very well constrained, but typical estimates are  $\xi_0 \simeq 0.75$  fm [27, 55]. Then  $\Delta t = a^4/\Gamma \simeq 0.32$  fm. Consider a critical endpoint at  $T_0 = 130$  MeV. A very rough estimate of the critical enthalpy density, based on non-interacting quarks and gluons, is  $w/(s_0 T_0) \simeq 11.2$  where  $s_0 = (\Delta t)^2/a^5$ . If we take the bare viscosity to be  $\eta/s = 1/(4\pi)$ , then the entropy in lattice units is given by  $\eta/\eta_0 = 0.5$ .

## IV. THEORETICAL EXPECTATIONS

### A. Statics

The static behavior of the model is governed by the partition function

$$Z = \int D\phi D\vec{\pi}^T \exp\left(-\frac{\mathcal{H}}{T}\right), \quad (56)$$

where  $\mathcal{H}$  is given in Eq. (4). There is no coupling between  $\phi$  and  $\vec{\pi}^T$  in the Hamiltonian, and the integral over the momentum density is Gaussian. This means that the equal time correlation function of  $\vec{\pi}^T$  is given by

$$\langle \pi_i^T(0, \vec{x}) \pi_j^T(0, \vec{x}') \rangle = T \rho P_{ij}^T \delta^3(\vec{x} - \vec{x}'). \quad (57)$$

This implies that the spectral density  $\langle \pi_i^T(0, \vec{k}) \pi_j^T(0, -\vec{k}) \rangle = P_{ij}^T \rho_\pi(\vec{k})$  is independent of  $\vec{k}$ , which is the classical equidistribution law.

The scalar field  $\phi$  is governed by a Hamiltonian in the universality class of the Ising model. This implies that for any value of  $\lambda$  we can tune  $m^2$  to a critical point  $m_c^2$  at which the theory becomes scale invariant. At the critical point the equal-time two-point function of  $\phi$  is

$$\langle \phi(0, \vec{x}) \phi(0, \vec{x}') \rangle \sim |\vec{x} - \vec{x}'|^{-d+2-\eta^*}, \quad \eta^* \simeq 0.0363 \quad (d=3), \quad (58)$$

where we have used  $\eta^*$  to distinguish the correlation function exponent from the viscosity  $\eta$ , and we have quoted the critical exponent determined in Ref. [63]. Away from the critical

point the correlation length is finite

$$\langle \phi(0, \vec{x}) \phi(0, \vec{x}') \rangle \sim \frac{e^{-|\vec{x}-\vec{x}'|/\xi}}{|\vec{x}-\vec{x}'|}, \quad \xi \sim |m^2 - m_c^2|^{-\nu}, \quad \nu \simeq 0.62999(5) \quad (d=3), \quad (59)$$

with the value of  $\nu$  taken from [64]. The integral of the two-point function defines the susceptibility

$$\chi = \int d^d x \langle \phi(0, \vec{0}) \phi(0, \vec{x}) \rangle, \quad \chi \sim |m^2 - m_c^2|^{-\gamma}, \quad \gamma = \nu(2 - \eta). \quad (60)$$

Note that the small value of  $\eta^*$  implies that the susceptibility is close to the mean field prediction  $\chi \sim \xi^2$ , and that the two-point function in momentum space is well described by the Ornstein-Zernike form  $\langle \phi(0, \vec{k}) \phi(0, -\vec{k}) \rangle \sim \xi^2 / (1 + (k\xi)^2)$ .

## B. Dynamics: Momentum density

The main new degree of freedom in model H is the momentum density  $\pi_i^T$  of the fluid. This dynamics of  $\pi_i^T$  can be accessed by studying the correlation function

$$C_{ij}(t, \vec{k}) = \left\langle \pi_i^T(0, \vec{k}) \pi_j^T(t, -\vec{k}) \right\rangle. \quad (61)$$

The transversality of  $\pi_i^T$  implies that  $C_{ij}(t, \vec{k}) = (\delta_{ij} - \hat{k}_i \hat{k}_j) C_\pi(t, k)$ . In linearized hydrodynamics this correlation function is governed by the shear mode and [4]

$$C_\pi(t, k) = \rho T \exp(-(\eta/\rho)k^2 t). \quad (62)$$

Non-linear effects will lead to a number of modifications of this result, even away from the critical point. The first is a renormalization of the viscosity due to hydrodynamic fluctuations and the self-advection of  $\pi_i^T$ , see Fig. 1(a). Here, we follow Ref. [10] and use a diagrammatic representation in which wavy lines represent Green functions of  $\pi_i^T$  and solid lines represent Green functions of  $\phi$ . A line with one arrow is a retarded Green function, and a line with two outgoing arrows represents a symmetric correlation function. The three-mode vertices correspond to the non-linear interaction terms in Eq. (1,2). Finally, the box-insertion in the correlation functions represents the strength of the noise in Eq. (5,6).

The renormalization of  $\eta$  was referred to as the ‘‘stickiness of sound’’ in Ref. [5, 65]. In the present case, we are not including sound modes and the stickiness of the fluid arises only

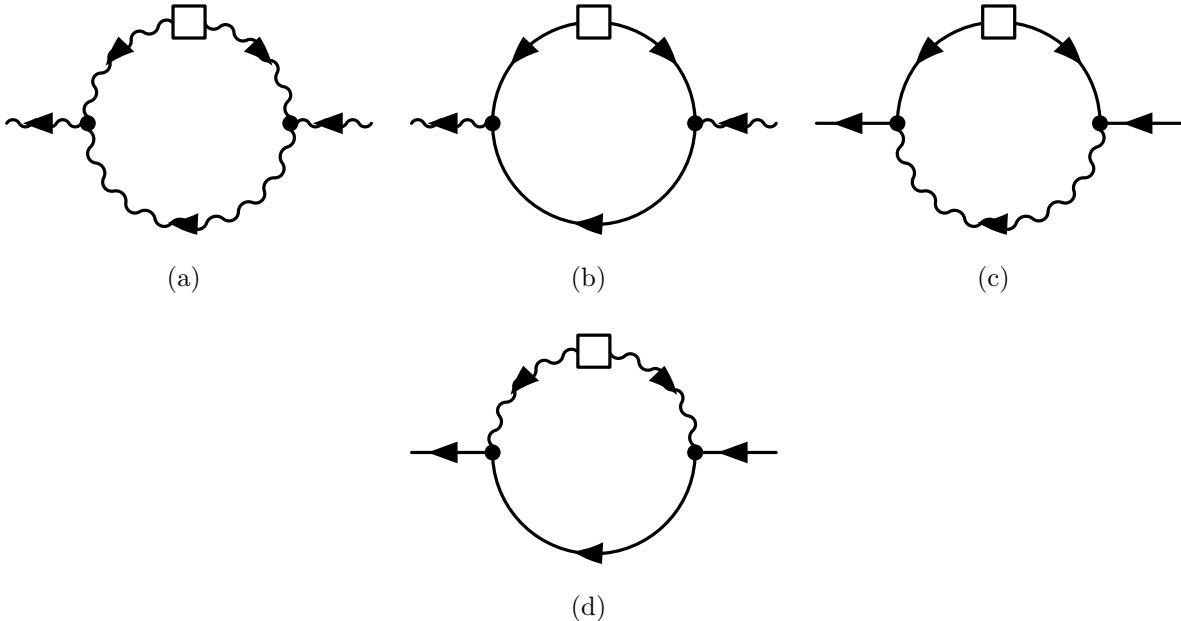


FIG. 1: Loop corrections to the retarded correlation function of hydrodynamic fluctuations. (a) Renormalization of the momentum correlation function by self-advection. (b) Renormalization of  $C_\pi$  due to the coupling between  $\pi$  and  $\phi$ . (c) and (d) Loop correction to the correlation function of  $\phi$  due to advection by  $\pi$ .

from the self-coupling of shear modes. Repeating the calculation [5, 65] for shear modes only gives

$$\eta_R = \eta + \frac{7}{60\pi^2} \frac{\rho T \Lambda}{\eta}, \quad (63)$$

where  $\eta$  is the bare viscosity,  $\eta_R$  is the renormalized viscosity, and  $\Lambda$  is a momentum-space cutoff. For a lattice regularized theory we expect  $\Lambda \simeq \pi/a$ , where  $a$  is the lattice spacing. This result has a number of interesting consequences. It implies that the renormalized viscosity cannot become arbitrarily small. As the bare viscosity is reduced, loop corrections become more important and eventually dominate over the bare viscosity. Of course, in this regime the one-loop approximation is no longer reliable. It is nevertheless instructive to estimate the minimum viscosity predicted by the one-loop calculation. We find

$$\eta_R|_{min} = \sqrt{\frac{7}{15\pi}} \sqrt{\frac{\rho T}{a}}, \quad (64)$$

which shows that the minimum kinematic viscosity scales inversely with the mass density of the fluid. The minimum viscosity is fluctuation-driven and increases with  $T$ . In the units adopted here,  $T = a = 1$ , we obtain  $\eta_R|_{min} \simeq 0.39\sqrt{\rho}$ .



Viscosity is also renormalized by the coupling to the scalar field, see Fig. 1(b). This diagram involves  $\phi\phi\pi_i^T$  vertices from both Eq. (1) and Eq. (2). The coupling in Eq. (2) is third order in gradients, and goes beyond the usual Navier-Stokes approximation. As a consequence, the renormalization of  $\eta$  by the coupling to the  $\phi$  field has not been studied before. We find that the  $(\nabla\phi)^2$  term in the free energy acts as an ultra-violet regulator, and the diagram is UV finite. The result is sensitive to the bare correlation length  $\xi^0 = m^{-1}$ . We obtain

$$\eta_R = \eta + \frac{1}{160\pi} \frac{T\xi^0}{\Gamma}. \quad (65)$$

For  $\xi^0 \sim a$  and  $a = \Gamma = T = 1$  we get  $\Delta\eta_R \simeq 0.002$ , which is a much smaller correction than Eq. (63).

The one-loop correction shown in Fig. 1(a) not only renormalizes the viscosity, but also qualitatively changes the long time behavior of the correlation function. The diagram in Fig. 1(a) corresponds to the splitting of a diffusive shear mode with wave number  $k$  into two modes with wave number  $k/2 \pm p$ . This gives a long time tail that scales as  $t^{-3/2} \exp(-D_\eta k^2 t/2)$ , where  $D_\eta = \eta/\rho$ . This tail is comparable to the tree level result in Eq. (62) for  $t > 3/(D_\eta k^2) \log(1/(t_0 D_\eta k^2))$ , where  $t_0$  is a microscopic time scale. In this regime higher loop corrections are not suppressed, and the correlation function becomes non-perturbative. Delacretaz conjectured that  $C_\pi \sim \exp(-\sqrt{\alpha D_\eta k^2 t})$  where  $\alpha$  is a constant that has to be determined non-perturbatively [9].

### C. Dynamics: Order parameter

The correlation function of the order parameter is

$$C_\phi(t, \vec{k}) = \langle \phi(0, \vec{k}) \phi(t, -\vec{k}) \rangle. \quad (66)$$

This correlation function can be used to define a wave-number dependent relaxation rate  $C(t, \vec{k}) \sim \exp(-\Gamma_k t)$ . A simple model for  $\Gamma_k$  was proposed by Kawasaki [66]

$$\Gamma_k = \frac{\Gamma}{\xi^4} (k\xi)^2 (1 + (k\xi)^2) + \frac{T}{6\pi\eta_R\xi^3} K(k\xi), \quad (67)$$

where the Kawasaki function is given by [56, 66]

$$K(x) = \frac{3}{4} [1 + x^2 + (x^3 - x^{-1}) \tan^{-1}(x)], \quad (68)$$

which satisfies  $K(x) \simeq x^2$  for  $x \ll 1$  and  $K(x) \simeq (3\pi/8)x^3$  for  $x \gg 1$ . The first term in Eq. (67) is the mean field relaxation rate in a purely diffusive theory (model B). It predicts that the relaxation rate of a fluctuation with wave number  $k = k^* \sim \xi^{-1}$  scales as  $\Gamma_{k^*} \sim \xi^{-4}$ , which corresponds to a dynamical critical exponent  $z = 4$ . This value is close to the non-perturbative result in model B,  $z = 4 - \eta$  (see Eq. (58)).

The second term in Eq. (67) comes from the coupling of the order parameter to the momentum density of the fluid, see Fig. 1(c) and (d). In the Kawasaki approximation this diagram is computed by assuming the damping rate of the shear mode to be of the form  $(\eta_R/\rho)k^2$ , and the damping rate of the order parameter to be of the mean field form,  $\Gamma k^2(\xi^{-2} + k^2)$ . In this approximation the diagrams in Fig. 1(c,d) are UV and IR finite, and the loop integral scales as  $\Gamma_k \sim T/(\eta_R \xi^3)$ . Equation (67) then predicts that the dynamical exponent  $z$  is equal to three. This is close to the result of a more systematic calculation in the  $\epsilon$ -expansion which, at two loops, predicts  $z \simeq 3.0712$  [67]. However, compared to the  $\epsilon$ -expansion the Kawasaki approximation has the virtue of giving a simple prediction for the wave number dependence of the relaxation rate. At small  $(k\xi)$  we have  $\Gamma_k \sim k^2$ , and at large  $(k\xi)$  we expect  $\Gamma_k \sim k^3$ .

Once the full relaxation rate  $\Gamma_k$  has been determined, one can go back and check the assumption that shear modes are damped as  $(\eta_R/\rho)k^2$ . This amounts to computing the diagrams in Fig. 1(b) with the Kawasaki expression for  $\Gamma_k$ . The result is [12]

$$\eta_R = \eta \left[ 1 + \frac{8}{15\pi^2} \log(\xi/\xi_0) \right], \quad (69)$$

which implies that the viscosity diverges at the critical point as  $\eta_R \sim \xi^{x_\eta}$  with  $x_\eta = 8/(15\pi^2) \simeq 0.054$ . This result is also close to that of the  $\epsilon$ -expansion, which predicts (at two loops)  $x_\eta \simeq 0.071$  [67]. The main observation is that  $x_\eta$  is very small, so that the divergence in  $\eta_R$  is weak, and the Kawasaki approximation is approximately self-consistent.

Finally, we note that there is a more physical argument that supports the prediction  $z \simeq 3$ . This argument can be found in the review of Hohenberg and Halperin [12], who attribute it to Arcovito et al. [15]. First, we observe that in the regime  $k\xi < 1$  the relaxation rate in Eq. (67) scales as  $\Gamma_k \sim k^2$ . This means that we can define a renormalized conductivity  $\Gamma_R$  by the relation  $\Gamma_k = \Gamma_R \chi^{-1} k^2$ . The critical scaling of  $\Gamma_R$  defines a new scaling exponent  $\Gamma_R \sim \xi^{x_\Gamma}$  [77]. The Kawasaki approximation predicts  $x_\Gamma = 1$ .

The second part of the argument is the observation that there is a physical picture that

constrains  $x_\eta + x_\Gamma$ . Consider a non-zero external field  $h(x)$ . Gradients of  $h(x)$  will drive a diffusive current  $\vec{j} = -\Gamma_R \vec{\nabla} h$ . However, in a fluid we can also have convection. The mechanical force per unit volume is  $\vec{f}_{mech} = -\phi \vec{\nabla} h$ , and this force can act coherently in a volume  $V \sim \xi^d$  controlled by the correlation length. The force  $\vec{f}_{mech}$  is balanced by Stokes drag  $\vec{f}_{visc} \sim \eta_R \xi^{d-2} \vec{v}$ , where  $\vec{v}$  is the drift velocity of the volume element. The forces balance if  $\vec{v} \sim -(\phi \xi^2 / \eta_R) \vec{\nabla} h$ , and the resulting current is  $\vec{j} \sim -(\phi^2 \xi^2 / \eta_R) \vec{\nabla} h$ . Finally, the mean value of  $\phi^2$  in the volume element is  $\phi^2 \sim \chi / \xi^d$ , and the convective current corresponds to a singular contribution to the conductivity  $\Gamma_R \sim (\chi / \eta_R) \xi^{2-d}$ . Using the scaling of  $\Gamma_R, \eta_R$  and  $\chi$  with the correlation length we obtain

$$x_\Gamma + x_\eta = 4 - d - \eta^* . \quad (70)$$

We note that this result is consistent with the Kawasaki approximation. Furthermore, if  $x_\eta$  and  $\eta^*$  are small, then  $x_\Gamma \simeq 4 - d - \eta^* \simeq 1$  (in  $d = 3$ ).

The final step in the argument is to note that  $x_\Gamma$  can be related to the dynamical exponent  $z$ . For this purpose we match the behavior of the relaxation rate at small  $(k\xi)$ ,  $\Gamma_k \simeq \Gamma_r \chi^{-1} k^2$ , to the result at large  $(k\xi)$ , which is  $\Gamma_k \simeq k^z$ . Consistency for  $(k\xi) \sim 1$  requires

$$z = 4 - x_\Gamma - \eta . \quad (71)$$

Combining Eq. (70) and (71) gives  $z = d + x_\eta$ , and for  $x_\eta \simeq 0$  we obtain  $z \simeq d$ .

## V. RESULTS

We have simulated the algorithm described in Sect. III on cubic lattices of size  $L^3$ . The algorithm is essentially local, and the computational cost for performing a single time step scales as  $L^3$ . However, near a second order phase transition critical slowing down implies that of order  $L^z$  time steps are required to equilibrate the system. In practice, near the critical point, we have been limited to lattices with  $L^3 \lesssim 64^3$  points. Away from the critical point, or for simulations that are not close to equilibrium, much larger lattices are possible. Examples of scalar field configurations encountered in model H simulations at and below the critical point are shown in Fig. 2.

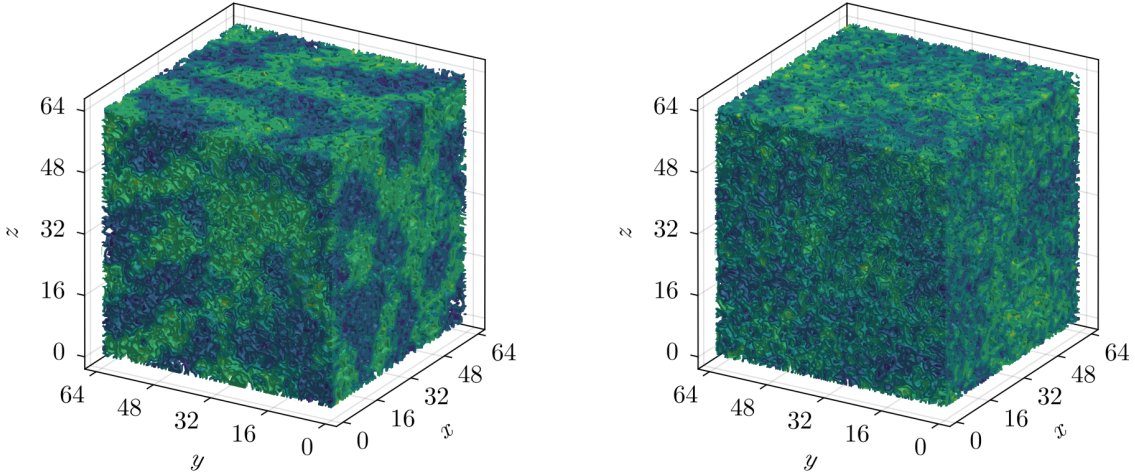


FIG. 2: Three-dimensional renderings of the order parameter  $\phi(\vec{x}, t)$  on a lattice  $\vec{x} = \vec{n}a$  with volume  $V = (La)^3$  where  $L = 64$ . The left figure is obtained from a model H simulation below the critical temperature  $m^2 = m_c^2 - 1.1$ , and the right from a simulation near the critical point. Green/blue colors correspond to positive/negative values of  $\phi$ .

### A. Static properties

The algorithm described in Section III D is designed to ensure that the equilibrium distribution  $P[\phi, \pi_i^T] \sim \exp(-\mathcal{H}[\phi, \pi_i^T]/T)$  is only governed by the Hamiltonian, and does not depend on the transport coefficients or the Poisson bracket terms. The Hamiltonian contains no coupling between the  $\phi$  and  $\pi_i^T$  fields, and as a result the equilibrium distribution of  $\phi$  that emerges from the model H equations of motion (1,2) is expected to be the same as the distribution obtained in model A [44] and model B [46]. Here, model A is described by purely relaxational dynamics and model B is governed by diffusion, but both models share the same Ising part of the Hamiltonian  $\mathcal{H}$ . In a finite volume there is a difference between the model A distribution and the result in model B/H because the model A dynamics does not conserve  $\phi$ . As a consequence, in model B/H the integral of  $\phi$  over the simulation volume cannot fluctuate.

Given that the static correlation functions of  $\phi$  are the same in model A/B/H we can

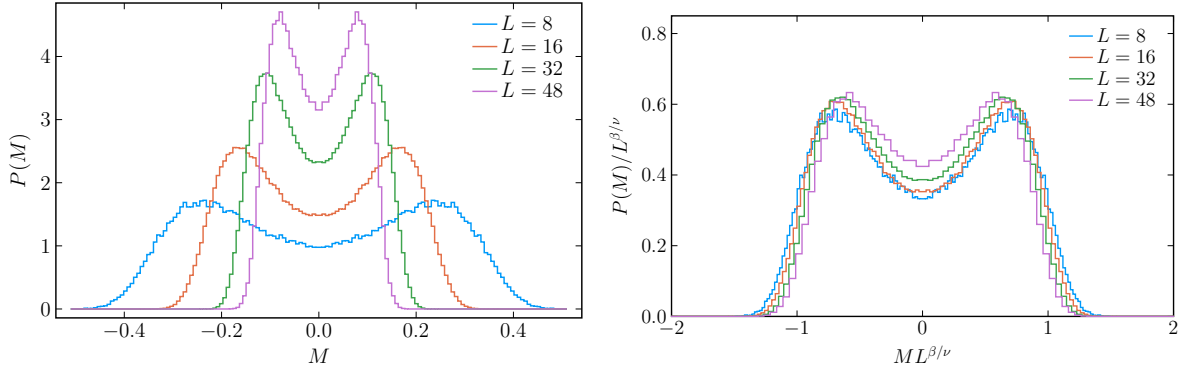


FIG. 3: The left panel shows the histogram of the magnetization  $M$  at the critical point  $m^2 = m_c^2$  in model A for four different volumes  $L = 8, 16, 32$  and  $48$ . The figure in the right panel demonstrates that the histogram scales with the exponent  $\beta/\nu$ .

determine the location of the critical point using whichever dynamics is the most convenient. In practice the main characteristic of the time evolution is the dynamical critical exponent  $z$ . The dynamical exponent is smallest in model A,  $z \simeq 2$ , which implies that this dynamical theory is the easiest to thermalize. In our previous work we determined the critical  $m_c^2$  (for  $\lambda = 4$ ) by calculating Binder cumulants in model A [44]. The cumulants are defined by [68]

$$U = 1 - \frac{\langle M^4 \rangle}{3\langle M^2 \rangle^2}, \quad (72)$$

where the magnetization  $M$  is defined as

$$M = \frac{1}{L^3} \sum_{\vec{x}} \phi(\vec{x}). \quad (73)$$

Binder cumulants are distinguished by the fact that at the infinite volume critical point  $m_{c,\infty}^2 \equiv m_c^2(L \rightarrow \infty)$  the leading finite volume corrections to  $U$  cancel. We can then determine  $m_{c,\infty}^2$  by locating the point where the finite volume cumulants cross. Furthermore, the critical value of  $U$  is universal and has been determined in high-precision simulations [69]. Using this input we obtained  $m_{c,\infty}^2 = -2.28587(7)$ . A histogram of the magnetization at the critical point in model A is shown in Fig. 3. We observe that the distribution for different volume  $V = L^3$  shows data collapse when the distribution is plotted as a function of  $ML^{\beta/\nu}$ , where  $\beta \simeq 0.326$  is the order parameter exponent, and  $\nu \simeq 0.630$  is the correlation length exponent.

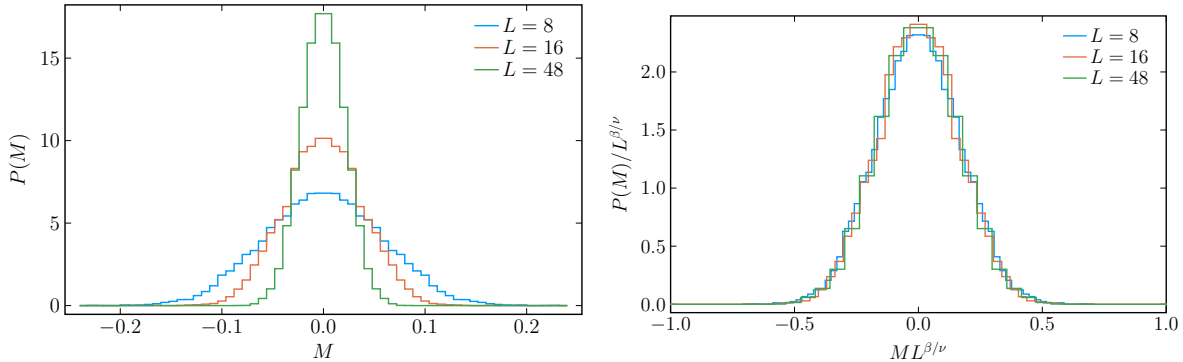


FIG. 4: The left panel shows the histogram of sub-volume magnetization  $M$  (integrated over half the simulation volume) at the critical point in model B for several different volumes. The distribution looks very different from that for model A in Fig. 3, but the scaling exponent is unchanged, as shown in the right panel.

In model B/H the total magnetization is conserved (typically we simulate at  $M = 0$ ), and the Binder cumulants are difficult to compute. In principle one can study  $M$  in some sub-volume, but then new finite volume corrections due to charge conservation appear. In our prior work on model B we studied the correlation length and relaxation time as a function of  $m^2 - m_{c,\infty}^2$ , and confirmed that the critical point is the same in model A and B dynamics [46]. This is supported by the results given in Fig. 4 which shows a histogram of the subvolume magnetization in model B at the critical point. We observe that the model B histograms differs significantly from the order parameter distribution in model A. We find, however, that scaling with  $ML^{\beta/\nu}$  and the same critical exponents is satisfied.

In model H we have observed a small shift in the critical value of  $m_c^2$ . This is likely related to the fact that the model H advection step described in Section III B does not exactly conserve the potential energy of  $\phi$ . As a consequence, the equilibrium value of  $\langle \phi^2 \rangle$  is shifted by the advection step. In Fig. 5 we show the static correlation function

$$C(x) = \langle \phi(0, t) \phi(\vec{x}, t) \rangle \quad (74)$$

in models B and H [78] We observe that a small shift,  $\delta m_c^2 = -0.03$  is required to reproduce the model B correlator using model H dynamics.

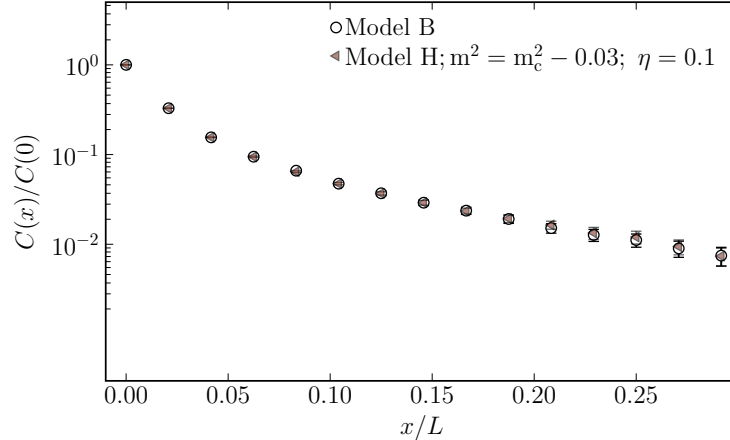


FIG. 5: Static correlation function of the order parameter  $C(x) = \langle \phi(0, t) \phi(\vec{x}, t) \rangle$  in model B and model H. We observe that a small shift in  $m_c^2$  is required to reproduce the static model B correlation function in model H.

### B. Dynamic correlation function of the momentum density

We first consider the two-point function of the momentum density defined in Eq. (61). An example is shown in Fig. 6 which shows the logarithmic derivative of  $C_\pi$  in model H for two different bare viscosities,  $\eta = 0.01$  and  $0.05$ . We observe a well-defined plateau that can be used to extract the physical viscosity. We have performed similar calculations for a range of values of  $\eta$  in a number of different theories. These include:

1. Model H as defined by Eqs. (1,2). The discretized form of the advection terms is given in Eqs. (41,42), and the dissipative terms are defined in Eqs. (47-52).
2. Model H0, which we have defined as Model H without the self-advection term in Eqs. (2) and (42). As discussed in Sect. IIB, model H0 is a consistent truncation of model H which is expected to be in the same dynamical universality class.
3. Pure self advection, which takes into account the non-linear dynamics of the momentum density, but ignores the coupling between  $\phi$  and  $\vec{\pi}^T$  in Eqs. (1,2) and Eqs. (41,42). In this theory the momentum density is decoupled from the critical dynamics of the order parameter.
4. Pure momentum diffusion, which corresponds to ignoring all mode couplings. In this

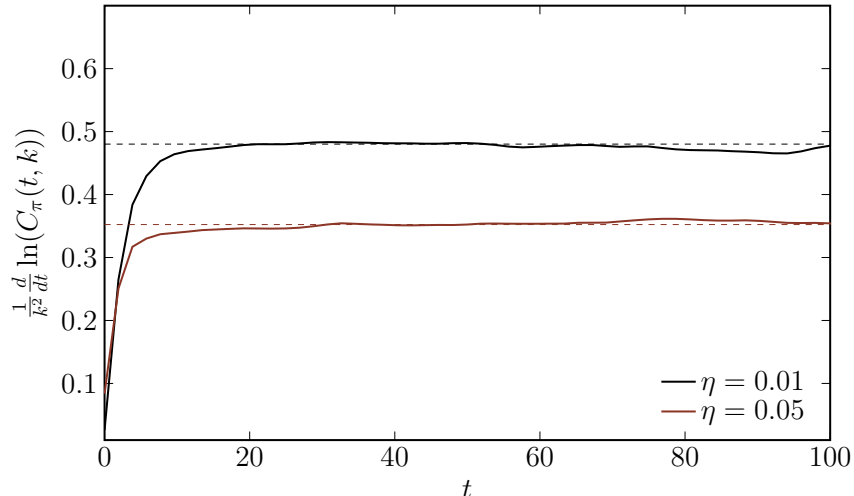


FIG. 6: Logarithmic derivative  $k^{-2}d \log C_\pi(t)/dt$  of the two-point function of the momentum density  $C_\pi(t, \vec{k})$  for the lowest momentum mode on a lattice of size  $L^3 = 48^3$ . The calculation was performed in model H for two different values of the bare viscosity,  $\eta = 0.01$  and  $0.05$ . The dashed lines show the extracted value of the viscosity.

approximation, the equation of the momentum density is completely linear.

The last of these theories, pure momentum diffusion, only serves as a very basic check of our numerical procedure. Indeed, the open circles in Fig. 7 show that the physical viscosity is very close to the bare viscosity. Pure self-advection takes into account the non-linear self coupling of the momentum density. In this case we observe a very significant renormalization of the viscosity. The blue triangles in Fig. 7 show that the physical viscosity tracks the bare viscosity down to  $\eta \gtrsim 0.5$ , but then it levels off and increases slightly for  $\eta \lesssim 0.1$ . This behavior is consistent with the one-loop renormalization shown in Fig. 1(a) and Eq. (63). Indeed, even though the one-loop calculation is not reliable once the correction is comparable to the tree level term [79] the observed viscosity minimum is quantitatively described by the estimate  $\eta_R|_{min} \simeq 0.39\sqrt{\rho}$  given in Sect. IV B.

The green squares in Fig. 7 show that the renormalization of the viscosity in model H0 is much smaller than the effect in model H or in a theory that includes only self-advection of the momentum density. This is consistent with the expectations presented in Sect. IV B, where we argued that the renormalization of  $\eta$  due to the coupling of  $\vec{\pi}^T$  to itself, Eq. (63), is much bigger than that due to the coupling to  $\phi$ , see Eq. (65). Note that the observed



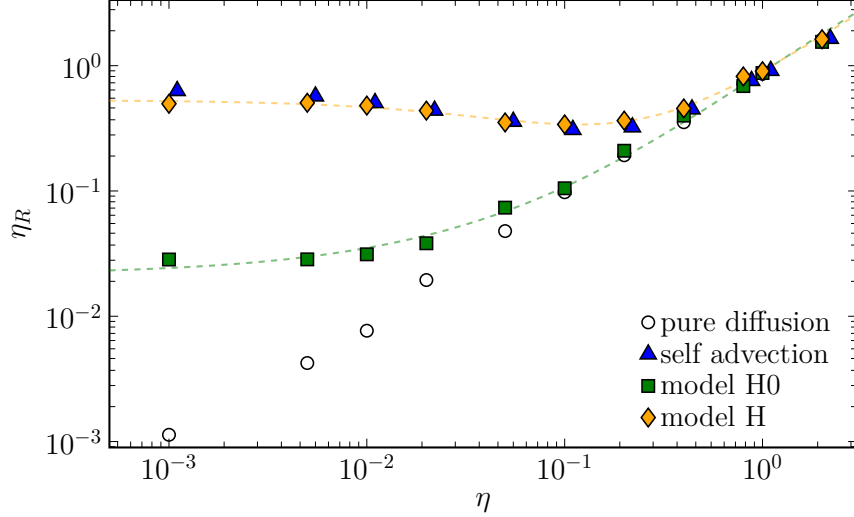


FIG. 7: Physical viscosity as a function of the bare viscosity in four different theories: 1) Model H at the critical point. 2) Model H0 at criticality (mutual advection of  $\phi$  and  $\vec{\pi}_T$  only). 3) Pure self-advection ( $\pi^T$  only couples to itself). 4) Pure momentum diffusion (no mode-couplings). The results were obtained on a lattice of size  $V = L^3$  with  $L = 48$ , and the fluid density was taken to be  $\rho = 1$ . Self advection results are offset horizontally to improve readability. The dashed lines show fits of the numerical data for model H0 and model H.

minimum in the viscosity,  $\eta_R \simeq 3 \cdot 10^{-2}$ , is somewhat bigger than the prediction in Eq. (65). This may be related to the fact that Fig. 7 shows the model H0 viscosity at the critical point, whereas Eq. (65) refers to the non-critical background. Mode-coupling theories, as well as the  $\epsilon$ -expansion, predict a weak critical divergence in the model H0 viscosity, see Eq. (69). For the parameters considered here, critical effects are expected to lead to a multiplicative renormalization of order  $\sim 10\%$ . This effect may well be present for  $\eta \lesssim 0.1$ , but it is difficult to disentangle from the non-critical additive renormalization. Only a careful scaling analysis, comparing different volumes as we will do in Sect. VC, can be used to identify the critical scaling of  $\eta_R$  [80]. Finally, the yellow diamonds in Fig. 7 show the physical viscosity in model H [81]. We observe that  $\eta_R$  is dominated by the non-critical renormalization that is already present in the calculation with pure self-advection. Compared to that, any critical enhancement is very difficult to observe.

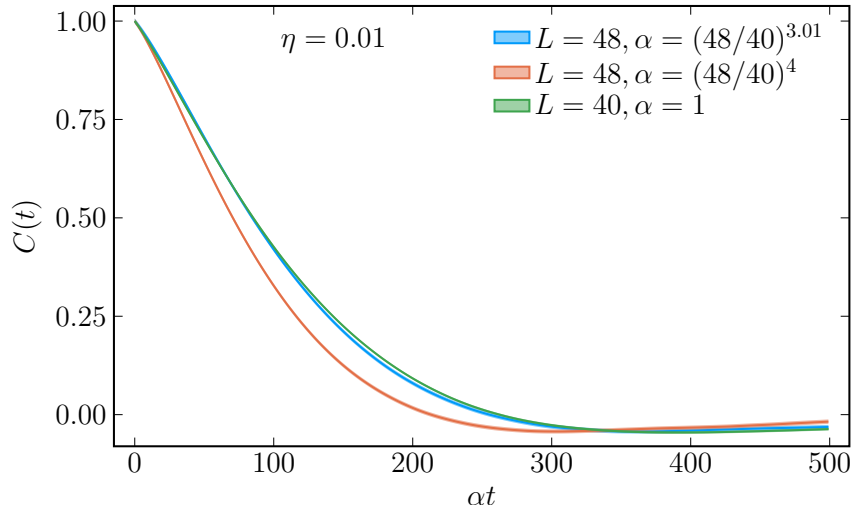


FIG. 8: Normalized dynamic order parameter correlation function  $C(t) = C_\phi(t, k_n)/C_\phi(0, k_n)$  for the second non-trivial momentum mode  $n = 2$  and for different values of  $L$  plotted as a function of the scaled time variable. This figure shows data taken at  $\eta = 10^{-2}$  for  $L = 40$  and  $48$ . Data collapse occurs for  $z \simeq 3.01$ , and the model B value  $z \simeq 4$  is clearly excluded.

### C. Dynamic scaling

In this section we study the dynamical scaling behavior of the order parameter correlation function  $C(t, \vec{k})$  defined in Eq. (66). Based on the discussion in Sect. IV C we expect that the relaxation rate is modified by the coupling to the momentum density, and that this coupling changes the scaling of the relaxation rate from  $\Gamma_k \sim \xi^{-4}$  to  $\Gamma_k \sim \xi^{-3}$ . The Kawasaki approximation given in Eq. (67) predicts that this crossover occurs for  $\xi \gtrsim (6\pi\Gamma\eta_R)/T$ , where  $\eta_R$  is the physical viscosity shown in Fig. 7. In model H we have  $\eta_R|_{min} \simeq 0.3$  and this condition is only marginally satisfied. Testing dynamical scaling is therefore simpler in model H0, where  $\eta_R$  can be as small as  $10^{-2}$ .

Fig. 8 shows a calculation of the order parameter correlation function in model H0 in two different volumes,  $L = 40$  and  $L = 48$ , with a bare viscosity  $\eta = 10^{-2}$  and  $\rho = 1$ . Dynamic scaling is the hypothesis that at the critical point the correlation function satisfies

$$C_\phi(t, k; L) = \tilde{C}_\phi(t/L^z, kL), \quad (75)$$

where  $\tilde{C}_\phi$  is a universal function, independent of  $L$ . Here, we have used the fact that at the critical point the correlation length  $\xi$  is only limited by the system size  $L$ . Away from

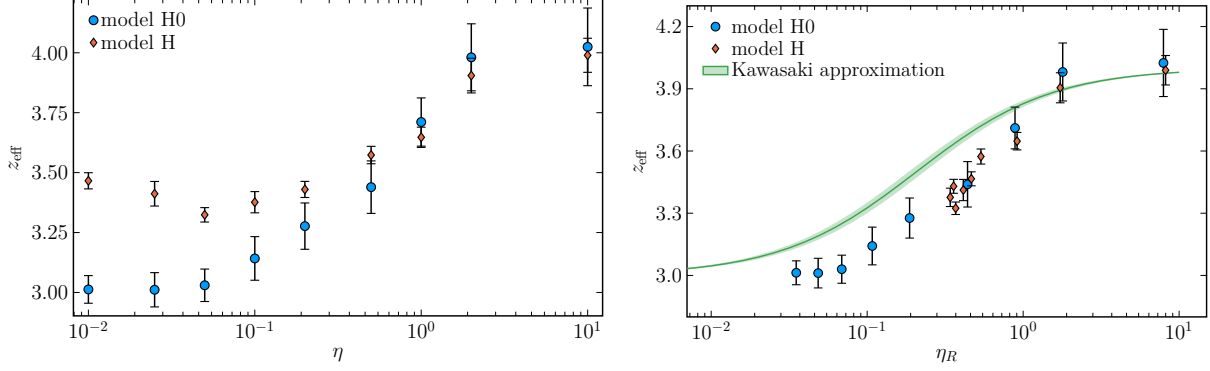


FIG. 9: Left panel: Dynamic scaling exponent  $z_{eff}$  extracted from the correlation function  $C(t, \vec{k})$  for different values of the bare and renormalized viscosity  $\eta$  in model H0 and H. We determined  $z_{eff}$  by comparing the correlation function for two different volumes,  $L = 40$  and  $48$ . We also show the prediction of the Kawasaki approximation, Eq. (67). The error band is defined by varying the correlation length in the range  $\xi \in [L/2\pi, L/2]$ . The right panel shows that  $z_{eff}$  is only a function of the physical viscosity.

the critical point, when  $a \ll \xi \ll L$ , the dynamical scaling relation in Eq. (75) holds with  $L$  replaced by  $\xi$ . In Fig. 8 we show  $C_\phi(t, \vec{k})$  for the second moment mode on the lattice,  $|\vec{k}| = 4\pi/L$ . This ensures that  $|\vec{k}|L$  remains fixed as  $L$  is varied. In the figure we look for dynamical scaling by plotting  $C_\phi(\alpha t, kL)$  with  $\alpha = 1$  for  $L = 40$  and  $\alpha = (40/48)^z$  for  $L = 48$ . We observe that dynamical scaling occurs for  $z = 3.01$ . The data clearly exclude a scaling exponent close to four.

We have repeated this calculation for a range of values of  $\eta$  in model H0. We extract an effective dynamical exponent  $z_{eff}$  by minimizing the normalized correlation function  $|C(t, L = 40) - C(\alpha t, L = 48)|$  with respect to  $\alpha = (40/48)^{z_{eff}}$  in the regime  $C(t) > 0.15$  (with  $C(0) \equiv 1$ ). The results are shown in Fig. 9. We also show the results in a complete model H calculation. For small values of the bare viscosity the extracted  $z_{eff}$  differs from the result in model H0. However, when plotted against the renormalized viscosity extracted in Fig. 7 the dynamic exponent in the two theories agrees (right panel in Fig. 9). For comparison, we also show the prediction of the Kawasaki approximation  $C(t, \vec{k}) \sim \exp(-\Gamma_k t)$  where the relaxation rate  $\Gamma_k$  is given in Eq. (67). The value of  $\xi$  at the critical point in a finite volume is not very well defined. In Fig. 9 we show the prediction of the Kawasaki approximation

for  $L/(2\pi) < \xi < L/2$ .

We observe that the effective dynamical exponent does indeed exhibit a crossover from  $z_{eff} \sim 4$  to  $z_{eff} \sim 3$ , and that this crossover is semi-quantitatively described by the Kawasaki approximation. For  $\eta_R = 10^{-2}$  we find  $z_{eff} = 3.013 \pm 0.058$ , which is our best estimate of the dynamical exponent in the infinite volume limit. This value is consistent with the prediction of the  $\epsilon$ -expansion at two loops,  $z \simeq 3.0712$  [67].

#### D. Two-dimensional fluids

In this section we study the behavior of a two-dimensional fluid near a critical point in the Ising universality class. There are several observations that motivate our study. The lower critical dimension of model  $H$  is  $d = 2$ , and interesting non-perturbative phenomena may take place in two-dimensional fluids. Also, the main source of theoretical information regarding the dynamical scaling exponents is the expansion around  $d = 4 - \epsilon$  dimensions, which is most questionable near  $d = 2$ . Calculations in  $d = 2$  may well be a good laboratory to compare numerical simulation, the  $\epsilon$ -expansion, and the functional renormalization group. Finally, two-dimensional fluids may have some relevance to the real world. For example, critical fluctuations in  $d = 2$  may control the critical dynamics of a fluid with rapid longitudinal expansion.

The static behavior of a two-dimensional fluid in the Ising universality class is well understood, both from theory and simulation. The free energy was determined by Onsager, and the correlation functions are governed by a well known two-dimensional conformal field theory [71]. The correlation function exponent is given by  $\eta^* = 0.25$ , and the correlation length exponent is  $\nu = 1$ . Less is known about the dynamics. The epsilon expansion predicts  $z = 2.179$  and  $x_\eta = 0.179$  [67]. Calculations based on the functional renormalization group find similar values of  $z$ , but either zero [22] or significantly smaller values [21] for  $x_\eta$ . A vanishing critical exponent for the shear viscosity can also be deduced from mode coupling approximation [72]. Note that there is a subtlety in trying to extract the viscosity of two-dimensional fluid. Even in a non-critical fluid there is a logarithmic divergence of the viscosity in the limit that the frequency goes to zero [9, 73, 74].

The algorithm described in Sect. III does not require any modifications in the two-dimensional case. In order to study critical dynamics we first have to locate the critical

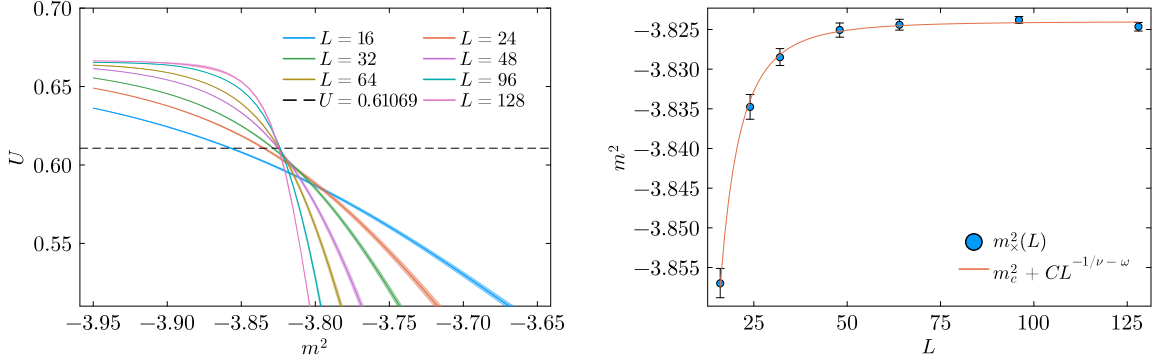


FIG. 10: Left panel: Binder cumulant for model A in two dimensions as a function of the control parameter  $m^2$  for different values of the system size  $L$ . The dashed line shows the critical value  $U^*$  of the Binder cumulant in the infinite volume limit [70]. Right panel: The figure shows the location  $m^2$  of the crossing points  $U(m^2, L) = U^*$  for different values of  $L$ , together with a fit of the form  $m^2 = m_c^2 + CL^{1/\nu-\omega}$ . Here,  $\omega = 2$  is a finite size scaling exponent. The fit yields  $m_c^2 = -3.8240 \pm 0.0003$ .

$m_c^2$ . As explained in Sect. V A this is most easily done using model A dynamics. The left panel of Fig. 10 shows the Binder cumulant  $U$  defined in Eq. (72) for different values of the system size  $L$  and the mass parameter  $m^2$ . The dashed line shows the known critical value of  $U$  in two dimensions,  $U^* = 0.61069$  [70]. The right panel shows the extrapolation to infinite  $L$ , which gives  $m_c^2 = -3.8240 \pm 0.0003$ . Following the procedure described in Sect. V A we have checked whether there is a small shift in  $m_c^2$  as we go from model A/B dynamics to model H. We find that the model H critical point is at  $m_c^2 \simeq -3.859$ .

Given the difficulty in extracting the shear viscosity of a two-dimensional fluid we have not attempted to study the renormalized viscosity in  $2d$ . In order to determine the dynamic scaling exponent we have computed the order parameter correlation function in Eq. (66) for a range of values of the bare viscosity. As in Sect. V C we look for dynamic scaling of the correlation functions computed for different values of  $L$ . In the left panel of Fig. 11 we show data collapse for the dynamic correlation function in two volumes with  $L = 40$  and  $L = 48$ . For  $\eta_0 = 10^{-2}$  we obtain  $z = 2.11 \pm 0.015$ , quite consistent with the prediction of the  $\epsilon$ -expansion quoted above,  $z = 2.179$ .

In the right panel of Fig. 11 we show the dependence of the value of  $z$  extracted in a finite volume on the bare viscosity. Similar to the results in three dimensions we observe

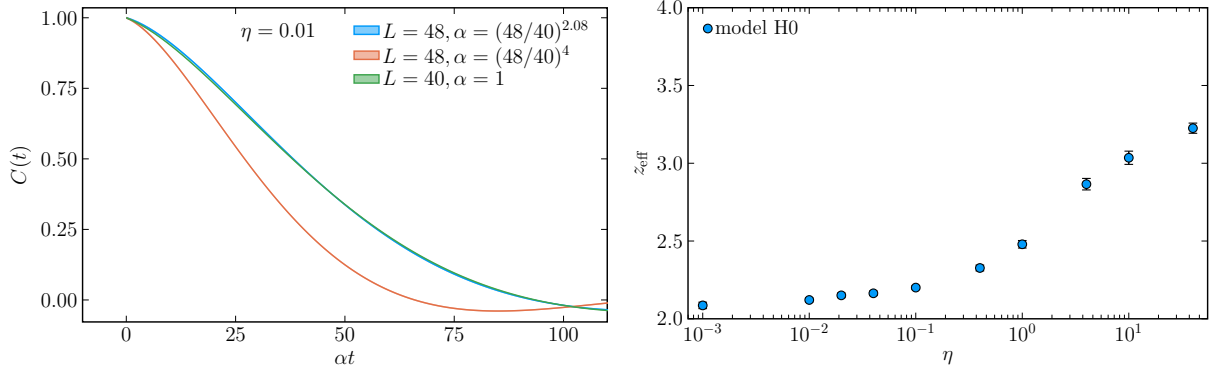


FIG. 11: Left panel: Dynamic scaling of the normalized order parameter correlation function  $C(t)$  for the second non-trivial momentum mode in model H0 in two dimensions, see Fig. 8 for the corresponding result in three dimensions. Right panel: Dynamic scaling exponent  $z_{eff}$  extracted from the correlation function  $C(t, \vec{k})$  for different values of the bare viscosity  $\eta$  in model H0 in  $d = 2$ .

a crossover, and the asymptotic value of  $z \simeq 2$  is only reached for very small values of  $\eta$ . Contrary to the three dimensional case we do not observe the model B value  $z \simeq 3.75$  for the largest values of  $\eta$  that we have explored. This is related to the fact that in two dimensions the value of  $\eta$  needed for the shear modes to decouple scales as  $\eta \sim \xi^2 T/\Gamma$ , compared to  $\xi T/\Gamma$  in three dimensions. Our algorithm becomes inefficient for very large values of  $\eta$ , and we have not studied values of  $\eta$  greater than  $10^2$ . We have verified that mean-field model B asymptotics is seen in smaller volumes.

## VI. SUMMARY AND OUTLOOK

We have studied a new approach to stochastic fluid dynamics which is based on a very simple and robust Metropolis algorithm. The main advantage of the algorithm is that fluctuation-dissipation relations are automatically satisfied, so that the simulation converges to an equilibrium distribution which is sampled from the desired microscopic free energy functional. We have used this method to compute the dynamic critical exponents of two and three-dimensional fluids near a critical endpoint in the universality class of the Ising model.

There are a number of issues that we would like to address in the future. One class

of problems involves improved calculations of the correlation function investigated in the present work. For example, what is the true long-time behavior of the momentum density correlation function? How can we best extract the macroscopic shear viscosity of the fluid? What is the best way to measure the scaling behavior of transport coefficients near the critical point? Addressing these issues may benefit from semi-analytical studies, for example based on Dyson-Schwinger equations or the functional renormalization group.

The second class of challenges has to do with making the simulations more realistic. This involves going to compressible fluid dynamics and including a realistic equation of state. In a compressible simulation we can study the behavior of the speed of sound, the sound attenuation rate, and the bulk viscosity. This is straightforward in principle, but we will have to study the renormalization of the equation of state.

Third, we would like to study non-trivial background flows, for example systems that undergo both longitudinal and transverse expansion. We are particularly interested in genuinely relativistic flows, in which the expansion velocity reaches a significant fraction of the speed of light. In this context it has recently been argued that the density frame formulation of hydrodynamics [47, 75] is particularly well suited for stochastic fluid dynamics and the Metropolis algorithm.

*Acknowledgments:* This work is supported by the U.S. Department of Energy, Office of Science, Office of Nuclear Physics through the Contracts DE-FG02-03ER41260, DE-SC0024622 and DE-SC0020081. This work used computing resources provided by the NC State University High Performance Computing Services Core Facility (RRID:SCR-022168), as well as resources funded by the Wesley O. Doggett endowment. We thank Andrew Petersen for assistance in working with the HPC infrastructure.

- 
- [1] T. Schäfer and D. Teaney, *Rept. Prog. Phys.* **72**, 126001 (2009), [arXiv:0904.3107 \[hep-ph\]](#) .
  - [2] S. Jeon and U. Heinz, *Int. J. Mod. Phys. E* **24**, 1530010 (2015), [arXiv:1503.03931 \[hep-ph\]](#) .
  - [3] P. Romatschke and U. Romatschke, *Relativistic Fluid Dynamics In and Out of Equilibrium*, Cambridge Monographs on Mathematical Physics (Cambridge University Press, 2019) [arXiv:1712.05815 \[nucl-th\]](#) .
  - [4] L. Landau and E. Lifshitz, *Course of Theoretical Physics: Statistical Physics, Part 2* (Perga-

- mon Press, 1980).
- [5] P. Kovtun, G. D. Moore, and P. Romatschke, *Phys. Rev. D* **84**, 025006 (2011), [arXiv:1104.1586 \[hep-ph\]](#) .
  - [6] M. Crossley, P. Glorioso, and H. Liu, *JHEP* **09**, 095 (2017), [arXiv:1511.03646 \[hep-th\]](#) .
  - [7] X. Chen-Lin, L. V. Delacrétaz, and S. A. Hartnoll, *Phys. Rev. Lett.* **122**, 091602 (2019), [arXiv:1811.12540 \[hep-th\]](#) .
  - [8] A. Jain and P. Kovtun, *Phys. Rev. Lett.* **128**, 071601 (2022), [arXiv:2009.01356 \[hep-th\]](#) .
  - [9] L. V. Delacretaz, *SciPost Phys.* **9**, 034 (2020), [arXiv:2006.01139 \[hep-th\]](#) .
  - [10] J. Chao and T. Schäfer, *JHEP* **01**, 071 (2021), [arXiv:2008.01269 \[hep-th\]](#) .
  - [11] G. Basar, (2024), [arXiv:2410.02866 \[hep-th\]](#) .
  - [12] P. C. Hohenberg and B. I. Halperin, *Rev. Mod. Phys.* **49**, 435 (1977).
  - [13] K. Rajagopal and F. Wilczek, *Nucl. Phys. B* **399**, 395 (1993), [arXiv:hep-ph/9210253](#) .
  - [14] D. T. Son and M. A. Stephanov, *Phys. Rev. D* **70**, 056001 (2004), [arXiv:hep-ph/0401052](#) .
  - [15] G. Arcovito, C. Faloci, M. Roberti, and L. Mistura, *Phys. Rev. Lett.* **22**, 1040 (1969).
  - [16] L. Canet and H. Chate, *J. Phys.* **40**, 1937 (2007), [arXiv:cond-mat/0610468](#) .
  - [17] L. Canet, H. Chate, and B. Delamotte, *J. Phys. A* **44**, 495001 (2011), [arXiv:1106.4129 \[cond-mat.stat-mech\]](#) .
  - [18] D. Mesterházy, J. H. Stockemer, L. F. Palhares, and J. Berges, *Phys. Rev. B* **88**, 174301 (2013), [arXiv:1307.1700 \[cond-mat.stat-mech\]](#) .
  - [19] Y.-r. Chen, Y.-y. Tan, and W.-j. Fu, *Phys. Rev. D* **109**, 094044 (2024), [arXiv:2312.05870 \[hep-ph\]](#) .
  - [20] J. V. Roth and L. von Smekal, *JHEP* **10**, 065 (2023), [arXiv:2303.11817 \[hep-ph\]](#) .
  - [21] Y.-R. Chen, Y.-Y. Tan, and W.-J. Fu, (2024), [arXiv:2406.00679 \[hep-ph\]](#) .
  - [22] J. V. Roth, Y. Ye, S. Schlichting, and L. von Smekal, (2024), [arXiv:2409.14470 \[hep-ph\]](#) .
  - [23] J. I. Kapusta, B. Muller, and M. Stephanov, *Phys. Rev. C* **85**, 054906 (2012), [arXiv:1112.6405 \[nucl-th\]](#) .
  - [24] S. Mukherjee, R. Venugopalan, and Y. Yin, *Phys. Rev. Lett.* **117**, 222301 (2016), [arXiv:1605.09341 \[hep-ph\]](#) .
  - [25] Y. Akamatsu, A. Mazeliauskas, and D. Teaney, *Phys. Rev. C* **95**, 014909 (2017), [arXiv:1606.07742 \[nucl-th\]](#) .
  - [26] M. Stephanov and Y. Yin, *Phys. Rev. D* **98**, 036006 (2018), [arXiv:1712.10305 \[nucl-th\]](#) .



- [27] Y. Akamatsu, D. Teaney, F. Yan, and Y. Yin, *Phys. Rev. C* **100**, 044901 (2019), [arXiv:1811.05081 \[nucl-th\]](#) .
- [28] X. An, G. Başar, M. Stephanov, and H.-U. Yee, *Phys. Rev. C* **100**, 024910 (2019), [arXiv:1902.09517 \[hep-th\]](#) .
- [29] X. An, G. Başar, M. Stephanov, and H.-U. Yee, *Phys. Rev. C* **102**, 034901 (2020), [arXiv:1912.13456 \[hep-th\]](#) .
- [30] X. An, G. Başar, M. Stephanov, and H.-U. Yee, *Phys. Rev. Lett.* **127**, 072301 (2021), [arXiv:2009.10742 \[hep-th\]](#) .
- [31] J. B. Bell, A. L. Garcia, and S. A. Williams, *Phys. Rev. E* **76**, 016708 (2007), [arXiv:math/0612324 \[math.NA\]](#) .
- [32] A. Donev, E. Vanden-Eijnden, A. Garcia, and J. Bell, *Communications in Applied Mathematics and Computational Science* **5**, 149 (2010), [arXiv:0906.2425 \[physics.flu-dyn\]](#) .
- [33] B. A. Camley and F. L. H. Brown, *Phys. Rev. Lett.* **105**, 148102 (2010), [arXiv:1105.4898 \[cond-mat.soft\]](#) .
- [34] F. Balboa, J. B. Bell, R. Delgado-Buscalioni, A. Donev, T. G. Fai, B. E. Griffith, and C. S. Peskin, *Multiscale Modeling & Simulation (SIAM)* **10**, 1369 (2012), [arXiv:1108.5188 \[physics.flu-dyn\]](#) .
- [35] C. Young, J. I. Kapusta, C. Gale, S. Jeon, and B. Schenke, *Phys. Rev. C* **91**, 044901 (2015), [arXiv:1407.1077 \[nucl-th\]](#) .
- [36] J. Berges, S. Schlichting, and D. Sexty, *Nucl. Phys. B* **832**, 228 (2010), [arXiv:0912.3135 \[hep-lat\]](#) .
- [37] D. Schweitzer, S. Schlichting, and L. von Smekal, *Nucl. Phys. B* **960**, 115165 (2020), [arXiv:2007.03374 \[hep-lat\]](#) .
- [38] D. Schweitzer, S. Schlichting, and L. von Smekal, *Nucl. Phys. B* **984**, 115944 (2022), [arXiv:2110.01696 \[hep-lat\]](#) .
- [39] M. Nahrgang, M. Bluhm, T. Schäfer, and S. A. Bass, *Phys. Rev. D* **99**, 116015 (2019), [arXiv:1804.05728 \[nucl-th\]](#) .
- [40] G. Pihan, M. Bluhm, M. Kitazawa, T. Sami, and M. Nahrgang, *Phys. Rev. C* **107**, 014908 (2023), [arXiv:2205.12834 \[nucl-th\]](#) .
- [41] V. A. Kuznietsov, O. Savchuk, M. I. Gorenstein, V. Koch, and V. Vovchenko, *Phys. Rev. C* **105**, 044903 (2022), [arXiv:2201.08486 \[hep-ph\]](#) .

- [42] A. Chen, E. H. Chimowitz, S. De, and Y. Shapir, *Phys. Rev. Lett.* **95**, 255701 (2005).
- [43] A. Florio, E. Grossi, A. Soloviev, and D. Teaney, *Phys. Rev. D* **105**, 054512 (2022), [arXiv:2111.03640 \[hep-lat\]](#) .
- [44] T. Schäfer and V. Skokov, *Phys. Rev. D* **106**, 014006 (2022), [arXiv:2204.02433 \[nucl-th\]](#) .
- [45] A. Florio, E. Grossi, and D. Teaney, *Phys. Rev. D* **109**, 054037 (2024), [arXiv:2306.06887](#) .
- [46] C. Chattopadhyay, J. Ott, T. Schäfer, and V. Skokov, *Phys. Rev. D* **108**, 074004 (2023), [arXiv:2304.07279 \[nucl-th\]](#) .
- [47] G. Başar, J. Bhambure, R. Singh, and D. Teaney, *Phys. Rev. C* **110**, 044903 (2024), [arXiv:2403.04185 \[nucl-th\]](#) .
- [48] C. Chattopadhyay, J. Ott, T. Schaefer, and V. V. Skokov, *Phys. Rev. Lett.* **133**, 032301 (2024), [arXiv:2403.10608 \[nucl-th\]](#) .
- [49] Y. Gao, K. Kirkpatrick, J. Marzuola, J. Mattingly, and K. A. Newhall, *Communications in Mathematical Sciences* **19**, 453 (2021), [arXiv:1806.05282 \[math.PR\]](#) .
- [50] R. Folk and H.-G. Moser, *J. Phys. A* **39**, R207 (2006).
- [51] X. An, G. Basar, M. Stephanov, and H.-U. Yee, *Phys. Rev. C* **108**, 034910 (2023), [arXiv:2212.14029 \[hep-th\]](#) .
- [52] P. Parotto, M. Bluhm, D. Mroczek, M. Nahrgang, J. Noronha-Hostler, K. Rajagopal, C. Ratti, T. Schäfer, and M. Stephanov, *Phys. Rev. C* **101**, 034901 (2020), [arXiv:1805.05249 \[hep-ph\]](#) .
- [53] M. Kahangirwe, S. A. Bass, E. Bratkovskaya, J. Jahan, P. Moreau, P. Parotto, D. Price, C. Ratti, O. Soloveva, and M. Stephanov, *Phys. Rev. D* **109**, 094046 (2024), [arXiv:2402.08636 \[nucl-th\]](#) .
- [54] A. Onuki, *Phys. Rev. E* **55**, 403 (1997).
- [55] M. Martinez, T. Schäfer, and V. Skokov, *Phys. Rev. D* **100**, 074017 (2019), [arXiv:1906.11306 \[hep-ph\]](#) .
- [56] A. Onuki, *Phase Transition Dynamics* (Cambridge University Press, 2002).
- [57] A. Vasil'ev, *The Field Theoretic Renormalization Group in Critical Behavior Theory and Stochastic Dynamics* (Chapman & Hall/CRC, 2004).
- [58] N. V. Antonov and A. N. Vasil'ev, *Theor. Math. Phys.* **60**, 671 (1984).
- [59] R. Folk and G. Moser, *Phys. Rev. E* **57**, 683 (1998).
- [60] I. E. Dzyaloshinskii and G. E. Volovick, *Annals of Physics* **125**, 67 (1980).

- [61] Y. Morinishi, T. Lund, O. Vasilyev, and P. Moin, *Journal of Computational Physics* **143**, 90 (1998).
- [62] C.-W. Shu and S. Osher, *Journal of Computational Physics* **77**, 439 (1988).
- [63] L. F. Alday and A. Zhiboedov, *JHEP* **06**, 091 (2016), [arXiv:1506.04659 \[hep-th\]](#) .
- [64] S. El-Showk, M. F. Paulos, D. Poland, S. Rychkov, D. Simmons-Duffin, and A. Vichi, *J. Stat. Phys.* **157**, 869 (2014), [arXiv:1403.4545 \[hep-th\]](#) .
- [65] C. Chafin and T. Schäfer, *Phys. Rev. A* **87**, 023629 (2013), [arXiv:1209.1006 \[cond-mat.quant-gas\]](#) .
- [66] K. Kawasaki, *Annals of Physics* **61**, 1 (1970).
- [67] L. T. Adzhemyan, A. Vasiliev, Y. S. Kabrits, and M. V. Kompaniets, *Theoretical and Mathematical Physics* **119**, 454 (1999).
- [68] K. Binder, *Zeitschrift fur Physik B Condensed Matter* **43**, 119 (1981).
- [69] M. Hasenbusch, K. Pinn, and S. Vinti, (1998), [arXiv:cond-mat/9804186](#) .
- [70] G. Kamieniarz and H. W. J. Blote, *Journal of Physics A: Mathematical and General* **26**, 201 (1993).
- [71] P. Francesco, P. Mathieu, and D. Senechal, *Conformal Field Theory*, Graduate Texts in Contemporary Physics (Springer New York, 2012).
- [72] T. Ohta, *Progress of Theoretical Physics* **54**, 1566 (1975).
- [73] L. P. Kadanoff, G. R. McNamara, and G. Zanetti, *Phys. Rev. A* **40**, 4527 (1989).
- [74] P. Kovtun, *J. Phys. A* **45**, 473001 (2012), [arXiv:1205.5040 \[hep-th\]](#) .
- [75] J. Armas and A. Jain, *SciPost Phys.* **11**, 054 (2021), [arXiv:2010.15782 \[hep-th\]](#) .
- [76] Note that we could have used the centered gradient of  $\phi$  in the dissipative step. However, this choice makes the stochastic update more non-local, and significantly increases the complexity of a checker board update. In practice, exactly conserving the centered derivative kinetic energy significantly improves conservation of the forward derivative kinetic energy.
- [77] Note that in the literature  $x_\Gamma$  is usually denoted by  $x_\lambda$ .
- [78] We compare model H to model B because the finite volume correction to  $C(x)$  due to charge conservation is the same in models B and H.
- [79] We have also not attempted to compute the diagram using a lattice regulator, and have instead used the simple estimate  $\Lambda = \pi/a$  to relate the continuum cutoff  $\lambda$  to the lattice spacing  $a$ .
- [80] Note that this will be difficult. In Sect. [VC](#) we compare  $L = 40$  and  $L = 48$ . Using  $x_\lambda \simeq 0.05$

as predicted by the  $\epsilon$ -expansion, the expected enhancement of  $\eta_R$  is  $(48/40)^{0.05} \approx 1.01$ , i.e. 1% difference between the curves, too small to be observed with high confidence.

[81] We have performed fits of the renormalized viscosity as a function of the bare one using the trial function  $\ln \eta_R = f(x = \ln \eta) = d[e \tanh(ax + b) - 1] + c(ax + b)[1 + \tanh(ax + b)]$ . The fit yields  $a = 0.28(0.53)$ ,  $b = 0.514(0.81)$ ,  $c = 1.138(0.87)$ ,  $d = 1.86(1.01)$  and  $e = 1(-0.372)$  for model H0 (model H).